Czech Technical University in Prague

Faculty of Electrical Engineering

Space Master

DIPLOMA THESIS

Modeling and control of a satellite's geostationary orbit

Department of Space Science, Kiruna Space Campus

LULEÅ UNIVERSITY OF TECHNOLOGY

Prague, 2007

Author: Kleanthis Neokleous

Declaration

I, Kleanthis Neokleous, declare that this diploma Thesis is my own work and has not been submitted in any form for another degree or diploma at any university or other institute.

Information derived from published and unpublished work of others has been acknowledged in the text and a list of references is given in the bibliography

In Prague on Signature

_____ _____

Acknowledgments:

I would firstly like to express my deep appreciation and thanks to all the people who helped me in any way in completing this Thesis work, but mostly my advisors Dr Ing. Jiri Roubal and Dr Ing. Petr Husek of the Czech Technical University, as well as Professor Andreas Johansson of the Luleå University of Technology. Moreover, I would also like to express my gratitude to Dr Zdeněk Hurák for his valuable advice in solving difficult technical problems.

I would like also to thank the Human Spaceflight, Microgravity and Exploration Programmes of the European Space Agency (ESA) for the financial support and the recourses provided.

Lastly, but not least I would like to thank my family, friends and colleagues for their patience and support during the last two years of the Spacemaster course.

Abstract

In this Thesis a complete model of the dynamics describing the orbit of a geostationary satellite has been developed by using the Euler- Hill equations of relative motion. Following that, a system has been developed to control the satellite's motion, which was the main objective of this work. Typically, this is classic problem in formation flight when the objective is to follow a "leader" or an analogous formation. On a similar basis, the idea developed and applied in this Thesis, was to control the satellite in order to minimize the distance from the satellite to the "leader" which in this case, is considered as a point orbiting in an ideal trajectory, irrespective of external or internal influences or disturbances. Real satellites are influenced by disturbances mainly caused from body forces due to the non-homogeneity and oblateness of the earth, body forces due to third-body interactions that generate satellite perturbations, mainly from the moon and the sun, and traction forces from solar radiation and solar wind. Consequently, models causing those disturbances were developed. Finally, the satellite's trajectory has been controlled using optimum and robust control design methods such as an LQ regulator and an H-infinity optimal control synthesis approach.

Table of contents

List of figures

Notation valid for all Chapters:

Scalars	- small *italic* letters	e.g	*a, b, c*, …
Functions	- CAPITAL non-italic letters	e.g	A, B, C, …
Vectors	- small **bold** non-italic letters	e.g	**a, b, c**, …
Matrices	- **CAPITAL bold** non-italic letters	e.g	**A, B, C**

Chapter 1

Description of the problem & derivation of relative equations of motion

Symbols for Chapter 1:

ρ_{moon} = Satellite's distance from the moon
ρ_{sun} = Satellite's distance from the sun
$\boldsymbol{F}_{grav}$ = Gravitational force
r = The orbit radius (from the center of the earth)
R_E = The equatorial radius of the earth
λ = The geocentric latitude of the orbit
Λ = The geocentric longitude of the orbit
μ = The earth's gravitational constant
Φ = Gravitational potential
P_l = Legendre polynomials
J_l = Zonal harmonics (dimensionless coefficients).
Ω = Right ascension of the ascending node
ω = Argument of perigee
i = Inclination of the orbit
M = $n(t-t_0)$ the mean anomaly, where n is the mean motion.
m_s = Satellites mass
m_{moon} = Moon's mass
γ_p = Acceleration caused by moon's gravitational field

1.1. Introduction

A common problem in the operation of satellites is to guide them and position them at a desired orbit. During its motion however, it is influenced by numerous forces of diverse intensities and directions, emanating from different sources. These forces tend to disturb the satellite and put it into other than the desired orbit.

In this chapter an analysis of the problems encountered in modeling and estimating the forces acting on a satellite will be made. Some basic concepts of the geostationary orbit will be described, which is the case to be studied for the work of this Thesis.

Following that, the derivation of the relative equations of motion will be presented. The relative equations of motion are based on the Hill's equations mainly used for formation flight. However, in the case to be studied, the "leader" can be considered as an ideal point. That would be the satellite's target. More detail analysis about the Hill's equations on formation flight, can be seen in Marcel J. Sidi "Spacecraft Dynamics and Control" [1]

1.2. The Geostationary orbit

In a geostationary orbit, there are two major stages that concern the control of a satellite's orbit. The first one is the transfer from the Geosynchronous transfer Orbit (GTO) to the Final Geostationary Orbit (GEO). The second stage is the so-called Mission Stage, which is generally expected to last more than ten years. In this Thesis only the second stage of the geosynchronous orbit will be studied.

The main objective of the work is to simulate a geostationary orbit of a satellite and apply suitable control schemes in order to keep it in the desired orbit, irrespective of external influences and resulting perturbations, using the minimum possible fuel consumption.

In the mission stage, the primary parameters of a satellite that change with time are the **inclination**, **eccentricity** and the **longitude**. Hence, the task of station-keeping at a geostationary orbit consists primarily of three adjustments.

1) Longitude (East-West) correction

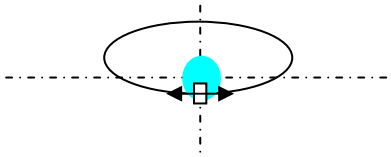

2) Inclination (North-South) correction

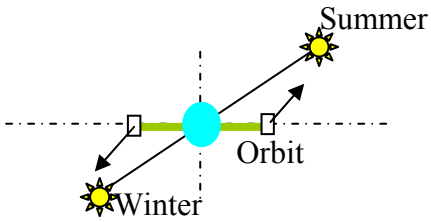

3) Eccentricity correction

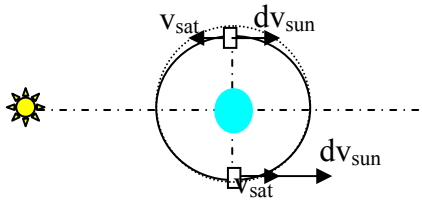

However, in the case of the relative motion (with respect to the desired orbit) those adjustments will be interpreted as *x*, *y* and *z* corrections in the rotating coordinate system that will be placed on the satellite as will be shown below.

In order to perform the desired control, it is necessary to model the equations of motion of the satellite. The Euler-Hill equations that describe the relative motion between satellites in neighboring orbits are commonly used.

By considering an ideal (desired) circular orbit of a point and having a real satellite orbit, the relative distance between any two points on the two orbits can be calculated through the use of the Euler-Hill equations for a dynamical system such as the satellite. The task then is to minimize this distance with the constraint of seeking minimum fuel consumption.

1.3 Generation of suitable data for an ideal geostationary orbit of a point.

Geosynchronous orbits are orbits with orbital period equal to the period of revolution of the earth about its axis of rotation. That is, in the ideal case when there are no perturbations, they have a constant angular speed ω = 1 rotation per day.
The geostationary orbits are geosynchronous, circular and equatorial. That is, their inclination and eccentricity are equal to zero.

The orbit of a satellite can be described by two non-linear coupled equations, which are obtained from an application of the fundamental equation of motion (Newton's 2nd Law).

$$\ddot{\mathbf{r}} = \mathbf{r}\dot{\theta}^2 - \frac{\mu}{r^2} + v_r$$

$$\ddot{\theta} = -\frac{2\dot{\mathbf{r}}\dot{\theta}}{r} + \frac{1}{r}v_\theta \qquad \text{1.1.a, b}$$

where,

r = Vector radius of the orbit

r = magnitude of the radius of the orbit, $r = |\mathbf{r}|$

θ = Angle of rotation

μ = GM, where G is the Universal Gravitational Constant and M is the mass of the earth.

v_θ, v_r = perturbations

A complete description of how those equations were derived will be explained and presented in detail in the main text of the Thesis. However, in the case of an **ideal geostationary orbit** with no disturbances, the basic equation of motion becomes

$$\ddot{\mathbf{r}}_1 = \mathbf{r}_1\dot{\theta}^2 - \frac{\mu}{r_1^2} = 0 \qquad \text{1.2}$$

That is, in the ideal case of a geostationary orbit, the angular velocity $\omega \equiv d\theta/dt$ is constant, as well as the velocity in the r_1 direction where r is the radius of the satellite's orbit.

thus, $\dot{\mathbf{r}}_1 = 0$ and $\dot{\boldsymbol{\omega}} = \ddot{\theta} = 0$

1.4 Generate data of a geostationary satellite orbit with perturbances

In the case of the real satellite, the equations of motion describing the orbit are given by equations 1.3.

$$\ddot{\mathbf{r}}_2 = \mathbf{r}_2\dot{\theta}^2 - \frac{\mu \mathbf{r}_2}{r_2^3} + \mathbf{f}$$

$$\ddot{\theta} = -\frac{2\dot{\mathbf{r}}_2\dot{\theta}}{r_2} \qquad \text{1.3.a, b}$$

where the vector $\mathbf{f} = \begin{bmatrix} f_x \\ f_y \\ f_z \end{bmatrix}$ includes the total forces acting on the satellite, that is, the disturbances and the thruster forces.

1.5 Derivation of the non-linear equations of relative motion.

In developing and applying the Euler-Hill equations [4], two coordinate systems are needed. An inertial coordinate system (geocentric) and a rotating coordinate system on the point of interest of the ideal orbit. A geocentric is a system that has fixed direction in space relative to the solar system. The Z axis is the axis of rotation of the earth in a positive direction, the X axis coincides with the vernal equinox vector, which is pointing to the sun on the 1st day of spring. The third axis Y completes an orthogonal right handed The local rotating coordinate system is placed on the orbiting point (*x, y, z*) as shown in Figure 1.1. In the local system, *x* is defined along the local vertical, z normal to the orbit plane and y completes a positive triad.

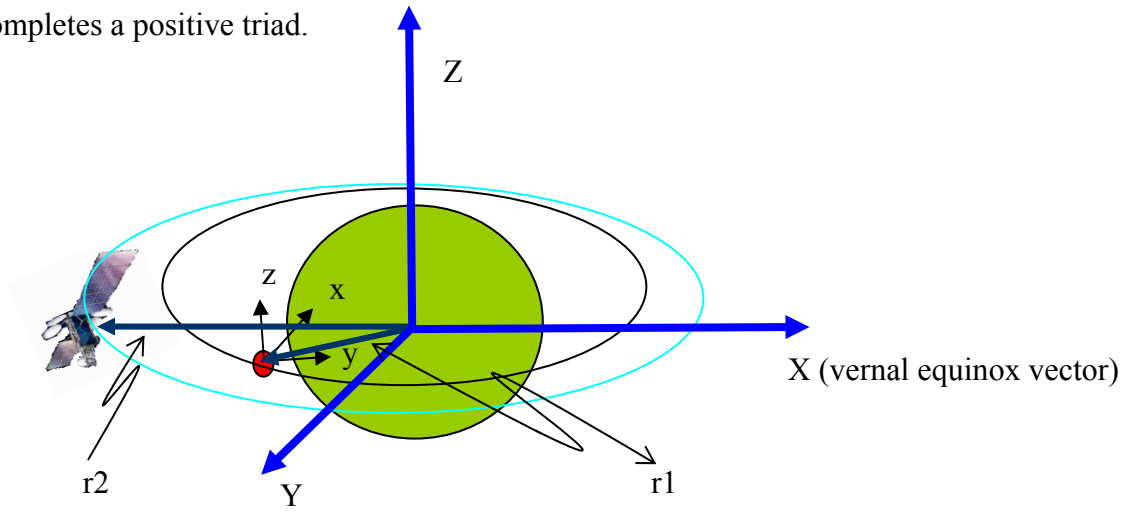

Figure 1.1.Local rotating coordinate system.

As mentioned above, the orbit of the point is described with equation 1.2 and the satellite's orbit with equation 1.3 and presented here again.

$$\ddot{\mathbf{r}}_1 = \mathbf{r}_1\dot{\theta}^2 - \frac{\mu\mathbf{r}_1}{r_1^3} \quad \text{and} \quad \ddot{\mathbf{r}}_2 = r_2\dot{\theta}^2 - \frac{\mu\mathbf{r}_2}{r_2^3} + \mathbf{f}$$

Let $\boldsymbol{\rho} = \mathbf{r}_1 - \mathbf{r}_2$,

$$\Rightarrow \ddot{\boldsymbol{\rho}} = \mathbf{a}_\rho = \mu\left[\frac{\mathbf{r}_1}{r_1^3} - \frac{\mathbf{r}_2}{r_2^3}\right] + \mathbf{f} \qquad 1.4$$

However, in the local rotating coordinate system, the vector equation of the relative distance ρ is as shown below. In this coordinate system, $\boldsymbol{\rho} = (x, y, z)^T$ and the acceleration is given by:

$$\ddot{\boldsymbol{\rho}} = \mathbf{a}_\rho = \frac{d^2\boldsymbol{\rho}}{dt^2} + 2\boldsymbol{\omega}\times\frac{d\boldsymbol{\rho}}{dt} + \frac{d\boldsymbol{\omega}}{dt}\times\boldsymbol{\rho} + \boldsymbol{\omega}\times\boldsymbol{\omega}\times\boldsymbol{\rho} \qquad 1.5$$

Where $\boldsymbol{\omega} = (0, 0, \dot{\theta})$ and $\dot{\theta}$ is the solution of equation 1.1 without the perturbances in the ideal orbit of the point.

By substituting **ω** and **r** in equation 1.5, and finally substituting in equation 1.4, we get the non linear equations of motion, where in the rotating system $\mathbf{r}_1 = (r_1, 0, 0)$.

$$\begin{aligned}
&\ddot{x} - 2\dot{\theta}\dot{y} - \ddot{\theta}y - \dot{\theta}^2 x = -\left(\frac{\mu(r_1 + x)}{\left((r+x)^2 + y^2 + z^2\right)}\right)^{3/2} + \frac{\mu}{r_1^2} \\
&\Rightarrow \ddot{y} + 2\dot{\theta}\dot{x} + \ddot{\theta}x - \dot{\theta}^2 y = -\left(\frac{\mu y}{\left((r+x)^2 + y^2 + z^2\right)}\right)^{3/2} \qquad 1.6 \\
&\ddot{z} = -\left(\frac{\mu(r_1 + x)}{\left((r+x)^2 + y^2 + z^2\right)}\right)^{3/2}
\end{aligned}$$

This model is referred to as the **true model** and the simulations conducted using this model, are referred to as **the complete nonlinear simulations.**

1.6 Derivation of the linear Euler-Hill equations.

By making the assumption that the distance between the reference point and the real orbit is small, equation 1.4 can be rewritten as

$$\ddot{\boldsymbol{\rho}} = \mathbf{a}_{\boldsymbol{\rho}} = \frac{\mu}{r_1^3}\left[\mathbf{r}_1 - \frac{r_1^3}{r_2^3}\mathbf{r}_2\right] + \mathbf{f} \qquad 1.7$$

Now,

$$\frac{\mathbf{r_2}}{r_2^3} = \frac{\boldsymbol{\rho} + \mathbf{r_1}}{\left(r_1^2 + 2\mathbf{r_1}\boldsymbol{\rho} + \boldsymbol{\rho}^2\right)^{3/2}} \qquad 1.8$$

Using a Taylor Series expansion,

$$\frac{\mathbf{r_2}}{r_2^3} = \frac{\boldsymbol{\rho} + \mathbf{r}_1}{r_1^3}\left[1 - \frac{3}{2}\left(\frac{2\mathbf{r}\boldsymbol{\rho}_1}{r_1^2}\right)\right] + O\left(\boldsymbol{\rho}^2\right) \qquad 1.9$$

By substituting in equation 1.7 and with $\frac{\mathbf{r_1}}{r_1} = (1,0,0)$ we get,

$$\mathbf{a}_{\boldsymbol{\rho}} = \frac{\mu}{r_1^3}\begin{bmatrix} 2x \\ -y \\ -z \end{bmatrix} + \mathbf{f} \qquad 1.10$$

Finally, introducing equation 1.4 into 1.10 we get the equations of motion.

$$\dot{\mathbf{v}} = \begin{bmatrix} 2(\mu/r_1^3) + \dot{\theta}^2 & \ddot{\theta} & 0 \\ -\ddot{\theta} & \dot{\theta}^2 - (\mu/r_1^3) & 0 \\ 0 & 0 & -(\mu/r_1^3) \end{bmatrix}\mathbf{x} + \begin{bmatrix} 0 & 2\dot{\theta} & 0 \\ -2\dot{\theta} & 0 & 0 \\ 0 & 0 & 0 \end{bmatrix}\mathbf{v} + \begin{pmatrix} f_x \\ f_y \\ f_z \end{pmatrix} \qquad 1.11$$

Where $\mathbf{x} = (x, y, z)^T$ is the vector of the relative position of the real satellite and $\mathbf{v} = \left(\dot{x}, \dot{y}, \dot{z}\right)$ is the velocity vector.

These are the **general linearized relative equations of motion for a Keplerian system**. It is pointed that these relative equations of motion are valid for both circular and elliptic leader orbits.

In the case however, where the reference orbit is circular, the Euler-Hill equations are derived.

Setting $n = \sqrt{\frac{\mu}{r_1^3}}$ to be the constant angular velocity of the reference orbit and $\ddot{\theta} = 0$, the final equations are:

$$\dot{\mathbf{v}} = \begin{bmatrix} 3n^2 & 0 & 0 \\ 0 & 0 & 0 \\ 0 & 0 & -n^2 \end{bmatrix} \mathbf{x} + \begin{bmatrix} 0 & 2n & 0 \\ -2n & 0 & 0 \\ 0 & 0 & 0 \end{bmatrix} \mathbf{v} + \begin{pmatrix} f_x \\ f_y \\ f_z \end{pmatrix} \qquad 1.12$$

$$\begin{aligned} \ddot{x} &= 2n\dot{y}(t) + 3n^2 x(t) + f_x \\ \ddot{y} &= -2n\dot{x}(t) + f_y \\ \ddot{z} &= -n^2 z(t) + f_z \end{aligned} \qquad 1.13$$

Chapter 2

Estimation of the forces acting on a satellite

Symbols for Chapter 2:

ρ_{moon} = Satellite's distance from the moon

ρ_{sun} = Satellite's distance from the sun

$\boldsymbol{F}_{grav}$ = Gravitational force

r = The orbit radius (from the center of the earth)

R_E = The equatorial radius of the earth

λ = The geocentric latitude of the orbit

Λ = The geocentric longitude of the orbit

μ = The earth's gravitational constant

Φ = Gravitational potential

P_l = Legendre polynomials

J_l = Zonal harmonics (dimensionless coefficients).

Ω = Right ascension of the ascending node

ω = Argument of perigee

i = Inclination of the orbit

M = $n(t-t_0)$ the mean anomaly, where n is the mean motion.

m_s = Satellites mass

m_{moon} = Moon's mass

γ_p = Acceleration caused by moon's gravitational field

2.1 Introduction

A satellite in space is subjected to external forces that tend to disturb and modify its desired orbit. The effect of these forces can be mild or serious, and consequent control action must be taken in order to keep the satellite at the desired path and attitude.

The external forces may be classified as **body** or **traction** forces. The body forces act on all the constituent mass elements of the satellite. The traction forces act on the external surface of the satellite.

There are many external sources for these forces, but the most important are the following four:

i) Body forces that are due to the varying gravity from the earth, which are mainly due to variations in the mass distribution and density (non-homogeneity) and to deviations of the earth's shape from a perfect sphere (oblateness).
ii) Body forces originating from large third-bodies.
iii) Traction forces from solar radiation and solar wind.
iv) Traction forces from small surrounding particles (atmospheric drag).

The atmospheric drag force is important at low-altitude orbits. For the geostationary orbit satellite that will be studied, where its altitude is in the order of 42164 km from the center of the earth, this kind of disturbance is not significant, and hence will not be included in the analysis.

A general description of the three major external forces acting on the satellite will follow and then a complete analysis on how these forces will influence the relative motion of the satellite in respect to the ideal point will be presented.
Finally, an analysis of the forces acting on the satellite by the thrusters will be presented.

2.2. Estimation of the external forces acting on a satellite

In this part of the chapter a general description of the forces due to the non-homogeneity and oblateness of the earth, from third body perturbations, from solar wind and from radiation will be developed.

2.2.1 Body forces due to the non-homogeneity and oblateness of the earth.

The disturbance caused by variations in the earth's gravitational field, is due to:

a) The fact that the mean shape of the earth is not a perfect sphere, but more like an ellipsoid on which local deformations are superimposed, and
b) To the non–homogeneous distribution of the earth mass.

There are various levels of detailing and modeling the gravitational forces. A brief description of the most significant models is described below.

The disturbance caused by the earths gravitational field, is due to the fact that the earth is not a perfect sphere. In actuality, the earth is more like an ellipsoid with local deformations.

If earth, could be modeled as a mass concentrated in a single point, or as a homogeneous sphere, then the gravitational potential would be given by the expression below [3].

$$\Phi(\mathbf{r}) = \frac{\mu}{\mathbf{r}} \qquad 2.1$$

$$\mathbf{F}_{grav} = \nabla\Phi(r) = -\frac{\mu}{r^3}\mathbf{r} \qquad 2.2$$

However, there are many irregularities in the earth's Gravitational Field, and these are modeled by a complex mathematics, in a system referred to as Potential Theory [1].

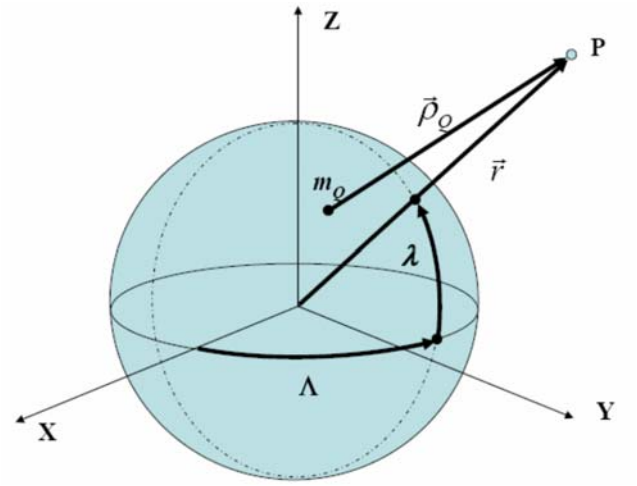

Figure 2.1.Gravitational force at a point due to a mass element

In Figure 2.1, each mass element m_Q in the earth is considered when determining the gravitational potential. The total effect from the distribution of these elemental masses is given by the potential function [1]:

$$\Phi(\mathbf{r},\Lambda,\lambda)=\frac{\mu}{\mathbf{r}}\left[1-\sum_{l=2}^{\infty}J_l\left(\frac{R_E}{\mathbf{r}}\right)^l P_l\sin(\lambda)+\sum_{l=2}^{\infty}\sum_{m=1}^{l}\left(\frac{R_E}{\mathbf{r}}\right)^l P_l\sin(\lambda)C_{lm}\cos(m\Lambda)S_{lm}\sin(m\Lambda)\right] \quad 2.3$$

where,

J_i	for $i = 2\ldots\infty$	Zonal harmonics
C_{lm}, S_{lm}	for l = m,	Sectorial harmonics
C_{lm}, S_{lm}	for $l \neq m \neq 0$,	Tesseral harmonics
P_l	Legendre Polynomials	
Λ,	Geocentric longitude	
λ	Geocentric Latitude,	

The **zonal harmonics**, J_i …, account for most of the earth's gravitational departure from a perfect sphere. This band and others reflect the earth's oblateness.

The **sectorial harmonics** take into account the extra mass distribution in the longitudinal regions.

The **tesseral harmonics** are primarily used to model earth deviations in specific regions, which depart from a perfect sphere.

For a body (planet) that has symmetry about the Z (polar) axis, i.e. has North/South symmetry, the form of the potential function (eq. 2.2) is significantly simplified, and is given by :

$$\Phi(\mathbf{r},\Lambda,\lambda)=\frac{\mu}{\mathbf{r}}\left[1-\sum_{l=2}^{\infty}J_l\left(\frac{R_E}{\mathbf{r}}\right)^l P_l\sin(\lambda)\right] \qquad 2.4$$

where,

P_l are the Legendre polynomials

$\boldsymbol{r}$ is the radius of the orbit

λ is the geocentric latitude of the orbit

J_l are dimensionless coefficients.

2.2.1.1 J_2 Effect (Non-Spherical Effect)

The largest perturbation due to the non-uniformity of the earth's mass is the J_2 component in the earth's geo-potential function given by:

$$\Phi(\mathbf{r},\Lambda,\lambda)=\frac{\mu}{\mathbf{r}}\left[1-J_2\left(\frac{R_E}{\mathbf{r}}\right)^2 P_2\sin(\lambda)\right] \qquad 2.5$$

where,

$$P_2\sin(\lambda)=\frac{1}{2}(3\sin\lambda^2-1) \qquad 2.6$$

is the second Legendre polynomial and $J_2 = 0.00108263$ [3].

The J_2 effect has a direct influence in the variation of the classical orbit parameters shown in the figure below.

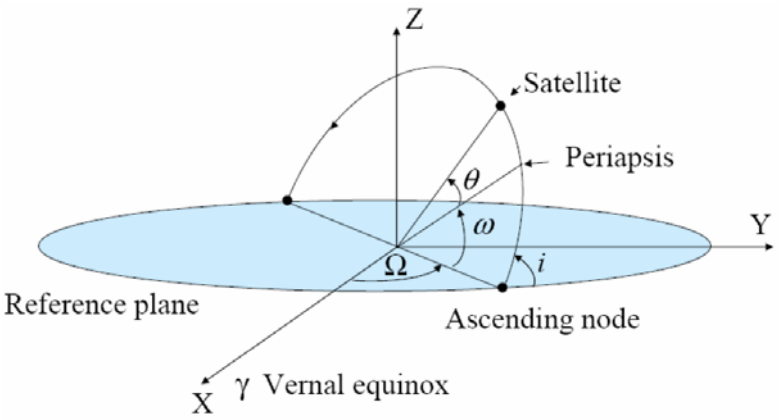

Figure 2.2 Basic orbit parameters

More specifically, the non-uniformity of the earth's mass has an influence in the variation of Ω, ω and M.

2.2.2 Forces due to Third-Body Perturbations

Other large body influences, can originate from planets, stars, and other stellar bodies. The most significant are the gravitational forces from the sun and the moon that cause periodic variations in all orbital elements, especially for high altitude orbits, such as the case of the geostationary orbit.

The sun and the moon can be treated as third bodies creating a perturbing force on an earth-orbiting satellite. Basically, this influence can be seen as the general case of the classic two-body problem.

In a system consisting of n interacting bodies, the sum of the forces acting on the ith body, will be:

$$\mathbf{F}_i = G\sum_{j=1}^{j=n} \frac{m_i m_j}{r_{ij}^3}(\mathbf{r_j} - \mathbf{r}_i) \qquad \{i \neq j\} \qquad 2.7$$

Substituting in the equation of Newton's second law of motion, $\mathbf{F} = m_i \frac{d^2\mathbf{r_i}}{dt^2}$, it follows that: $\frac{d^2\mathbf{r_i}}{dt^2} = G\sum_{j=1}^{j=n} \frac{m_j}{r_{ij}^3}(\mathbf{r_j} - \mathbf{r}_i) \qquad \{i \neq j\} \qquad 2.8$

If the specific case of perturbation caused by the moon's gravitational field, the perturbing acceleration can be calculated as below.

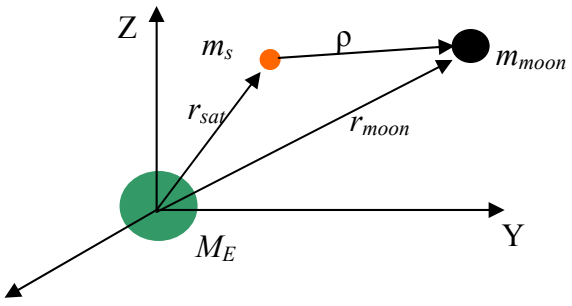

Figure 2.3.Third body perturbation

As can be seen in Figure 2.3, the origin of the inertial frame is located in the center of the earth. This leads to the final equation of the perturbing force caused by the moon as shown below.

$$\frac{d^2\mathbf{r_{sat}}}{dt^2} + G\frac{\mathbf{r_{sat}}}{r_{sat}^3}(M_E + m_s) = Gm_{moon}\left[\frac{\boldsymbol{\rho}}{\rho^3} - \frac{\mathbf{r_{moon}}}{r_{moon}^3}\right] \qquad 2.9$$

or

$$\ddot{\mathbf{r}}_{\mathbf{sat}} + G\frac{\mathbf{r_{sat}}}{r_{sat}^3}(M_E + m_s) = \boldsymbol{\gamma}_{\mathbf{p}} \qquad 2.10$$

where,

$\boldsymbol{\gamma}_{\mathbf{p}} = Gm_{moon}\left[\frac{\boldsymbol{\rho}}{\rho^3} - \frac{\mathbf{r_{moon}}}{r_{moon}^3}\right] = \mu_{moon}\left[\frac{\boldsymbol{\rho}}{\rho^3} - \frac{\mathbf{r_{moon}}}{r_{moon}^3}\right]$ is the perturbing acceleration.

It is interesting to mention that $\frac{\mu_{moon}}{r_{moon}^3}$ of moon is equal to $8.6\text{x}10^{-14}$ s^{-2}

and $\frac{\mu_{sun}}{r_{sun}^3}$ of the sun is equal to $3.96\text{x}10^{-14}$ s^{-2}

2.2.3 Forces due to the Solar Radiation and Solar wind

Solar radiation includes all the electromagnetic waves radiated by the sun, in a wide range of wavelengths from x-rays to radio waves.

The solar wind consists mainly of ionized nuclei and electrons, where both kinds of radiation may produce a physical pressure on the satellite's surface, and this pressure is proportional to the momentum flux of the radiation. That is, the momentum per unit area per unit time.

The mean solar energy flux integrated at the earth's position is given by:

$$F_e = \frac{1.358}{1.0004 + 0.034\cos(D)} \qquad \frac{W}{m^2} \qquad 2.11$$

where,

D is the phase of the year as calculated by starting on July 4th.

This is equivalent to a mean momentum flux of:

$P = F_e/c = 4.5\text{x}10^{-6}$ [kg.m^{-1}.s^{-2}] 2.12

where,

c is the velocity of light.

Finally, the solar radiation pressure F_R is proportional to P, to the cross-section area A of the satellite perpendicular to the sun line, and to a coefficient C_P that is dependent on the absorption characteristics of the satellite.

$F_R = PAC_P$ 2.13

where, C_p lies between 0 and 2.

For a perfectly absorbing material (black body), $C_p = 0$.

The solar radiation momentum flux effect on the perturbations of the orbit is much greater than that of the solar wind (by a factor of 100 to 1000), so the solar wind will not be considered as negligible compared to other effects.

2. 3 Perturbing Forces in the Relative Equations of Motion.

2.3.1 The J_2 effect

The Hill equations, in the linear form as derived previously, do not include the J_2 disturbance. So there is need of a set of linearized equations that are easy to use, but at the same time able to capture the J_2 effects.

A very interesting work was done in the MSc Thesis of Schweighart [2], where a new set of linearized equations of motion where developed. These equations are like Hill's equations in form, but also capture the effects of the J_2 disturbance force.

The basic idea of the analysis was to introduce the J_2 disturbance in the "real" satellites orbit equation as shown below.

$$\ddot{\mathbf{r}} = \frac{\mu}{r^2} + J_2(\mathbf{r}) = 0 \qquad 2.14$$

Where $J_2(\mathbf{r})$ is the force due to the J_2 disturbance [2] and $\mathbf{r}$ is the vector of the disturbed orbit.

The analysis of J_2 force is respect to the x and z axis of the rotating coordinate system on the point of the ideal orbit is given by,

$$\mathrm{J}_2(\mathbf{r}) = -\frac{3}{2}\frac{J_2 \mu R_E^2}{r^4}\left[(1-3\sin^2 i \sin^2\theta)x + (2\sin^2 i \sin\theta\cos\theta)y + (2\sin i \sin\theta\cos\theta)z\right] \quad 2.15$$

In the case of the geostationary orbit, the reference orbit to compare the relative motion is circular and equatorial.

Let $\boldsymbol{\rho}$ be defined as the relative vector $\mathbf{r_{ref}} - \mathbf{r}$.
Then, the next step in the derivation was to linearize both the standard gravitational term and the J_2 disturbance around this reference orbit.

$$\Rightarrow \ddot{\mathbf{r}} = \mathrm{g}(\rho_{\rho\varepsilon\phi}) + \nabla \mathrm{g}(\mathbf{r_{ref}})\bullet\boldsymbol{\rho} + J_2(\mathbf{r}) + \nabla J_2(\mathbf{r})\bullet\boldsymbol{\rho} \quad 2.16$$

An important note to be stated at this point is that under the influence of the J_2 disturbance force, the orbital planes rotate around the Z axis (the North Pole). This is due to the fact that the J_2 disturbance force is symmetric across the equator.

So, in the equatorial case, the linearized equations of motion correctly represent the out-of-plane motion, (the normal vector to the orbital plane).

Finally, as for the derivation of Hill's equations, in the local rotating coordinate system

$$\ddot{\boldsymbol{\rho}} = \ddot{\mathbf{r}}_{\mathbf{ref}} - \ddot{\mathbf{r}} + 2\boldsymbol{\omega}\times\frac{d\boldsymbol{\rho}}{dt} + \frac{d\boldsymbol{\omega}}{dt}\times\boldsymbol{\rho} + \boldsymbol{\omega}\times\boldsymbol{\omega}\times\boldsymbol{\rho} \quad 2.17$$

By substituting equation 2.2 into 2.3 and by defining $\boldsymbol{\omega}$ of the reference orbit, the final equations of relative motion are derived as presented below.

$$\begin{aligned} &\ddot{x} - 2nc\dot{y} - (5c^2-2)n^2 x = f_x \\ &\ddot{y} + 2n\dot{x} = f_y \\ &\ddot{z} + (3c^2-2)n^2 z(t) = f_z \end{aligned} \quad 2.18$$

where,

$$c = \sqrt{1 + \frac{3J_2 \mu R_E^2}{8 r_{ref}^{\ 2}} (1 + 3\cos 2i_{ref})}$$

An important observation is that if x, y and z relative initial are zero, then the perturbed orbit will never have a different x, y, z from the ideal orbit, if the only perturbance considered is from the J_2 effect.

The satellite's orbit can be seen in Figure 2.4.below where the only effect acting on the real satellite causing deviation from the ideal orbit is the J_2 effect. The time period were the evolution was made is for two days (≈2880 min).

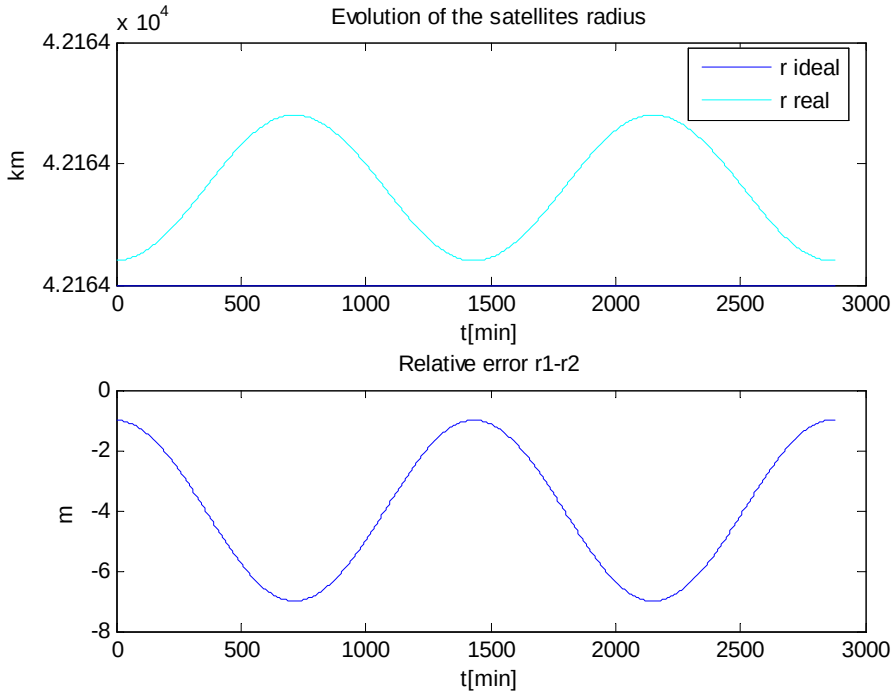

Figure 2.4.Evolution of the satellites radius as well as the relative error r1-r2 for the disturbance caused by the J_2 effect.

However, from what is mentioned above, equations 2.18 include only the disturbances due to the J_2 effect.The disturbances caused by the Sun and Moon gravitational effects causing the North South drift, are not included. In this case, a model was derived about the disturbances from the Sun and the Moon since those disturbances are dependent on the position of the earth and the position of the satellite with respect to the earth. Those models are described in the next paragraphs.

2.3.2 The Moon and Sun disturbance forces.

As pointed before, the satellite is influenced by perturbing forces from the earth, the sun and the moon. In order to calculate the direction of the force vector of every perturbance, the initial conditions of the position of the earth, moon and the satellite must be defined. For that, a specific day of the year should be considered, and that is the 21st of June. So, the position of the sun with respect to the earth can be defined by placing a coordinate system in the center of mass of the earth and having X axis the same as X equinox, Y axis pointing at the center of mass of the sun and X, Y on the ecliptic plane. The equatorial plane is inclined with respect to the ecliptic by 23.43^{o}

The position of the moon at this specific day of the year is in the X, Z plane of the coordinate system described above. That is by considering the earth as the center of our system then the Sun and moon have a 90^{o} angle difference. Finally, the moon's orbiting plane is inclined by 5.3^{o} from the ecliptic plane in the X direction. The satellite initial position is on the equatorial plane in the X direction. The positions described above are shown in Figure 2.5 below and should be considered as the initial conditions for the following calculations.

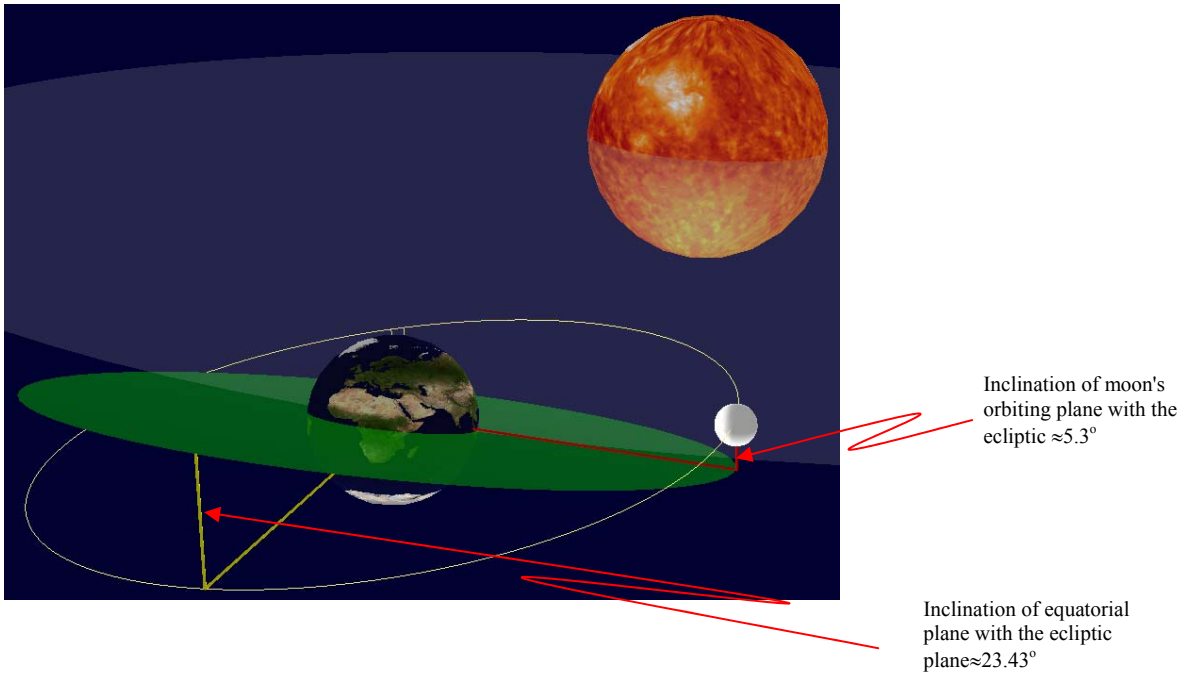

Figure 2.5.The three orbiting planes.

2.3.2.1 Moon disturbance

As described above, the moon's gravitational field causes an acceleration to the satellite. This acceleration, multiplied by the mass of the satellite equals the force acting on the satellite by the moon's gravitational field, as per the fundamental Newton's second law.

$$\Rightarrow F_{moon} = m_{sat}\boldsymbol{\gamma}_{\mathbf{p}}$$

However, since the moon and the satellite are both orbiting around the earth, the direction of the force vector is constantly changing.

So a model was created to calculate the amplitude and direction of the force vector acting by the moon to the satellite.

An effective approach in solving the problem of the combined movement of the moon and the satellite is to use spherical coordinates. That is, to assume that the moon is moving around the earth on the surface of a surrounding sphere. This can be visualized by thinking that the moon is orbiting in an approximately circular orbit around the center of mass of the earth and so is the satellite. So, by assuming that the satellite is stable, then it is the same like the moon is moving on a sphere.

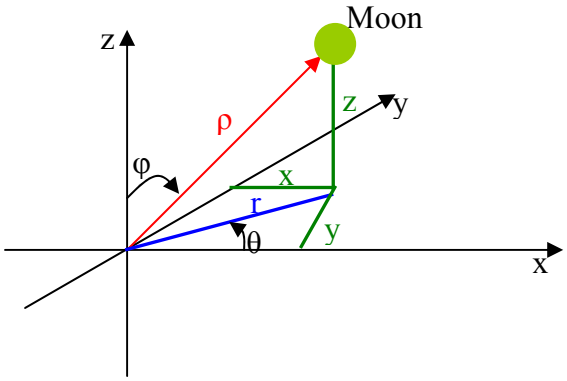

Figure 2.6.Spherical coordinates.

In Figure 2.6, if it is assumed that the green dot is the moon. Then, the position of the moon can be described by the three coordinates:

ρ The radial distance of a point from a fixed origin

φ The zenith angle from the positive z-axis

θ The azimuth angle from the positive x-axis.

Those coordinates, however, should be defined relative to the rotating coordinate system on the orbiting point.

In order for this to be done, a third coordinate system is placed on the rotating point. This coordinate system has the x_m axis pointing to the center mass of the moon and y_m axis is pointing to the sun on the ecliptic plane.

Then the x_m, y_m, and z_m of the moon can be defined relatively to the rotating coordinate system placed on the ideal orbiting point.

For that, three transformations need to be made in respect to the rotating coordinate system. The transformations are made from the coordinate system placed on the orbiting point to the moons coordinate system described above. Then the inverse transformation should be applied to get the moons coordinates in respect to the rotating coordinate system.

The first transformation is to go from the equatorial plane to the ecliptic. That is to rotate around x axis by 23.43°, as shown in figure 2.7.

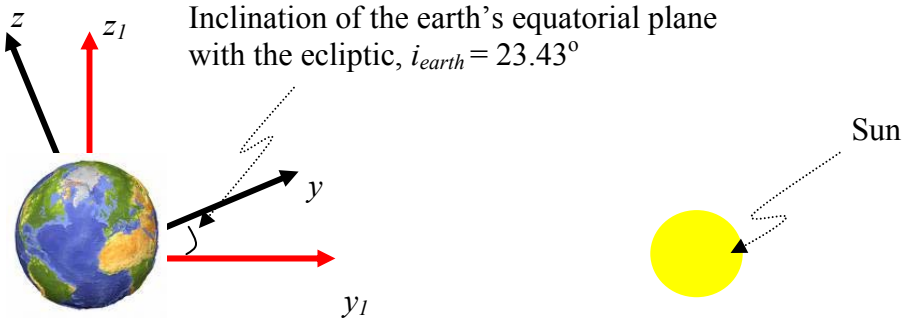

Figure 2.7.First transformation around x axis.

$$\Rightarrow \begin{bmatrix} x_1 \\ y_1 \\ z_1 \end{bmatrix} = \begin{bmatrix} 1 & 0 & 0 \\ 0 & \cos(i_{earth}) & \sin(i_{earth}) \\ 0 & -\sin(i_{earth}) & \cos(i_{earth}) \end{bmatrix} \begin{bmatrix} x \\ y \\ z \end{bmatrix} \qquad 2.19$$

The second transformation is a rotation of 5.3° around the y_2 axis. This can be seen in figure 2.8 where the sun is in the *y* direction. That is if we are watching figure 2.7 from behind the earth aligned with the sun.

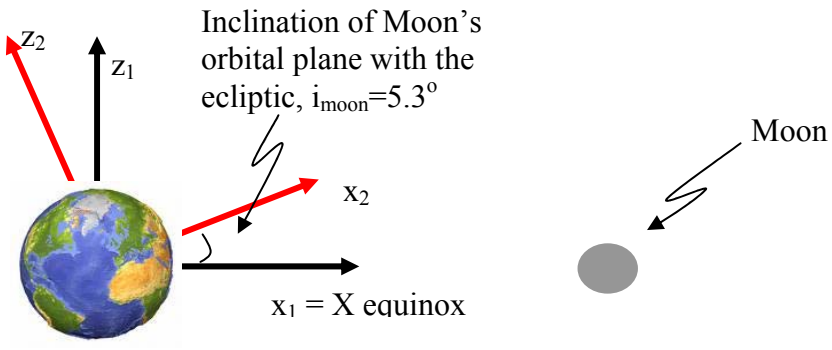

Figure 2.8.Second transformation around y axis.

$$\Rightarrow \begin{bmatrix} x_2 \\ y_2 \\ z_2 \end{bmatrix} = \begin{bmatrix} \cos(i_{moon}) & 0 & -\sin(i_{moon}) \\ 0 & 1 & 0 \\ \sin(i_{moon}) & 0 & \cos(i_{moon}) \end{bmatrix} \begin{bmatrix} x_1 \\ y_1 \\ z_1 \end{bmatrix} \qquad 2.20$$

Finally the third transformation is around the z axis of the rotating system equal with the moon's rotation angle, which is the integration of the moon's orbital period which is 28 days.

$$\Rightarrow \begin{bmatrix} x_3 \\ y_3 \\ z_3 \end{bmatrix} = \begin{bmatrix} \cos(\theta_{moon}) & \sin(\theta_{moon}) & 0 \\ -\sin(\theta_{moon}) & \cos(\theta_{moon}) & 0 \\ 0 & 0 & 1 \end{bmatrix}^{-1} = \begin{bmatrix} \rho_{moon} \\ 0 \\ 0 \end{bmatrix} \qquad 2.21$$

Where ρ_{moon} is the moon's distance with respect to the satellite. However, for simplification ρ_{moon} is considered from the earth's center of mass since the satellite's radii

compared to the moon's radii is very small. That is, to assume that the satellite is placed in the center of mass of the earth and rotating around itself.

Then *x*, *y* and *z* of the moon's coordinates with respect to the rotating coordinate system can be defined as below.

$$\begin{bmatrix} x \\ y \\ z \end{bmatrix} = \begin{bmatrix} 1 & 0 & 0 \\ 0 & \cos(i_{earth}) & \sin(i_{earth}) \\ 0 & -\sin(i_{earth}) & \cos(i_{earth}) \end{bmatrix}^{-1} \bullet \begin{bmatrix} \cos(i_{moon}) & 0 & -\sin(i_{moon}) \\ 0 & 1 & 0 \\ \sin(i_{moon}) & 0 & \cos(i_{moon}) \end{bmatrix}^{-1} \bullet \begin{bmatrix} \cos(\theta_{moon}) & \sin(\theta_{moon}) & 0 \\ -\sin(\theta_{moon}) & \cos(\theta_{moon}) & 0 \\ 0 & 0 & 1 \end{bmatrix}^{-1} = \begin{bmatrix} \rho_{moon} \\ 0 \\ 0 \end{bmatrix}$$

2.22

So, if the moon's coordinates are known, then the direction of the force vector by the moon to the satellite can be defined by the spherical coordinates.
From Figure 2.6,

$\phi = \cos^{-1}\left(\frac{z}{\rho_{moon}}\right)$ is the angle of the moon with respect to the z axis of the rotating system

and $\theta = \left[\tan^{-1}\left(\frac{y}{x}\right) - \theta_{sat}\right]$ is the angle of the moon with respect to the x axis of the rotating coordinate system.

Then,

$$F_x = \mathbf{F}\sin\phi\cos\theta$$
$$F_y = \mathbf{F}\sin\phi\sin\theta \qquad 2.23$$
$$F_z = \mathbf{F}\cos\phi$$

In Figure 2.9 below, the disturbance due to the moon's gravitational field is shown and the satellite's orbit as it deviates from the ideal orbit for a time period of two days.

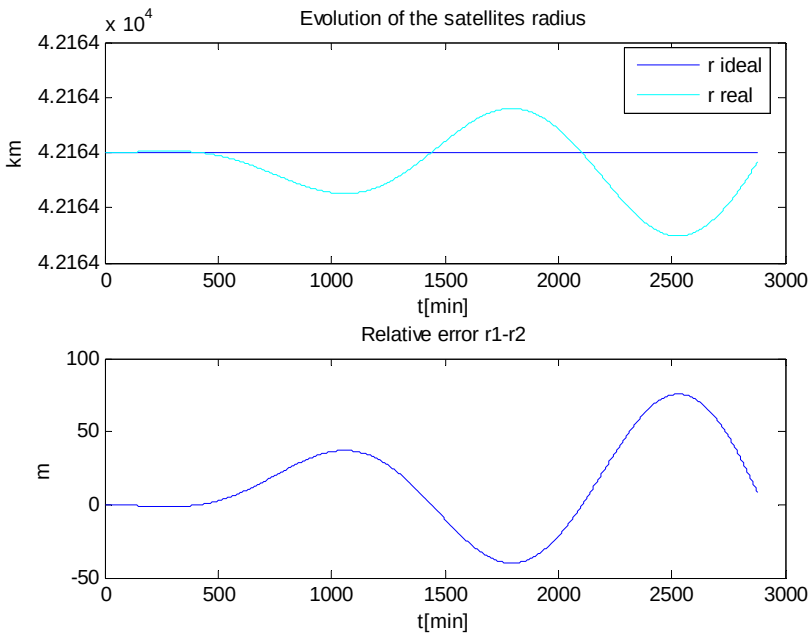

Figure 2.9.Evolution of the satellites radius as well as the relative error r1-r2 for the moon disturbance.

2.3.2.2 Disturbances from the sun

Similar procedure can be made for the calculation of the direction of the force vector from the solar pressure on the satellites area. In this case, a fourth coordinate system is introduced on the orbiting point, with the x axis equal to the rotating coordinate systems x axis and at the case of the initial conditions equal to x equinox and y axis pointing to the sun's center of mass. The z axis completes the orthogonal triad. Again the assumption that the orbiting point is in the center of the earth's mass is made. However, in this case the rotation of the earth around the sun was not taken into consideration, since the control calculations are for the maximum of one week.

Once again, the first transformation is to go from the equatorial plane to the ecliptic. That is to rotate around x axis by 23.43^{o}, as shown in Figure 2.7.

$$\Rightarrow \begin{bmatrix} x_1 \\ y_1 \\ z_1 \end{bmatrix} = \begin{bmatrix} 1 & 0 & 0 \\ 0 & \cos(i_{earth}) & \sin(i_{earth}) \\ 0 & -\sin(i_{earth}) & \cos(i_{earth}) \end{bmatrix} \begin{bmatrix} x \\ y \\ z \end{bmatrix} \qquad 2.24$$

The second transformation is a rotation around the *y* axis by the satellites rotation angle θ_{sat}. This would have been true if the satellite was stable and the Sun was orbiting around the satellite. So the rotation around the *z* axis should be -θ_{sat}

$$\Rightarrow \begin{bmatrix} x_2 \\ y_2 \\ z_2 \end{bmatrix} = \begin{bmatrix} \cos(-\theta_{sat}) & 0 & -\sin(-\theta_{sat}) \\ 0 & 1 & 0 \\ \sin(-\theta_{sat}) & 0 & \cos(-\theta_{sat}) \end{bmatrix} \begin{bmatrix} \rho_{sun} \\ 0 \\ 0 \end{bmatrix} \qquad 2.25$$

$$\Rightarrow \begin{bmatrix} Fx_{sun} \\ Fy_{sun} \\ Fz_{sun} \end{bmatrix} = \begin{bmatrix} 1 & 0 & 0 \\ 0 & \cos(i_{earth}) & \sin(i_{earth}) \\ 0 & -\sin(i_{earth}) & \cos(i_{earth}) \end{bmatrix}^{-1} \bullet \begin{bmatrix} \cos(-\theta_{sat}) & 0 & -\sin(-\theta_{sat}) \\ 0 & 1 & 0 \\ \sin(-\theta_{sat}) & 0 & \cos(-\theta_{sat}) \end{bmatrix}^{-1} \begin{bmatrix} F_{sun} \\ 0 \\ 0 \end{bmatrix} \qquad 2.26$$

In Figure 2.10 below, the disturbance due to the sun's gravitational field is shown and how the satellites orbit is deviated from the ideal orbit, again for a time period of two days.

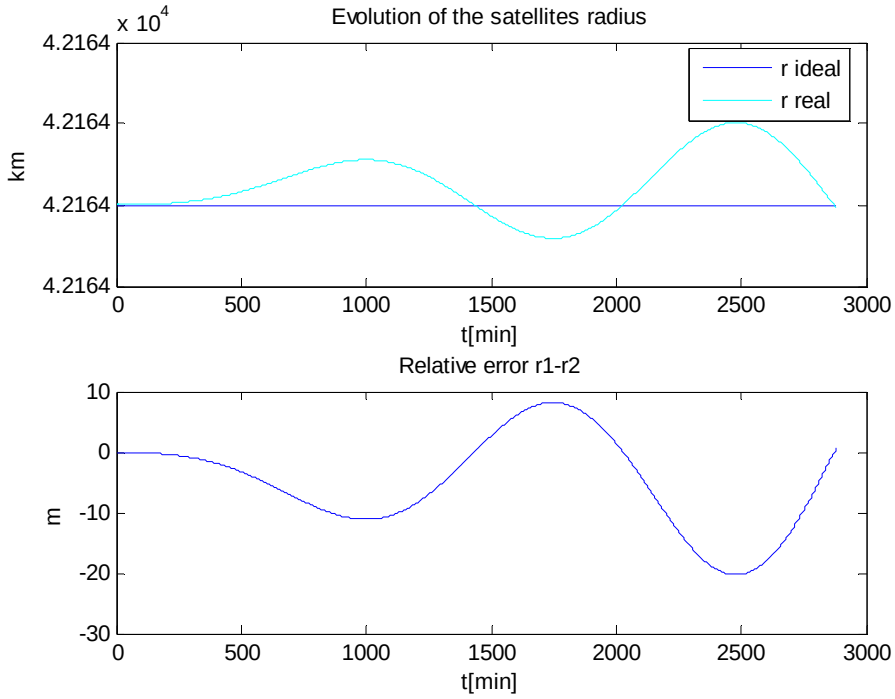

Figure 2.10.Evolution of the satellites radius as well as the relative error r1-r2 for the sun disturbance.

2.4. SIMULINK model of the system and the perturbing forces

Finally a complete model of the satellite dynamics was developed in MATLAB - SIMULINK, including the perturbances described previously.

This model can be seen in Figure 2.11 below, where the moon and sun perturbing force are calculated outside the block that computes the relative motion, and the J_2 disturbance is included in the equations of relative motion.

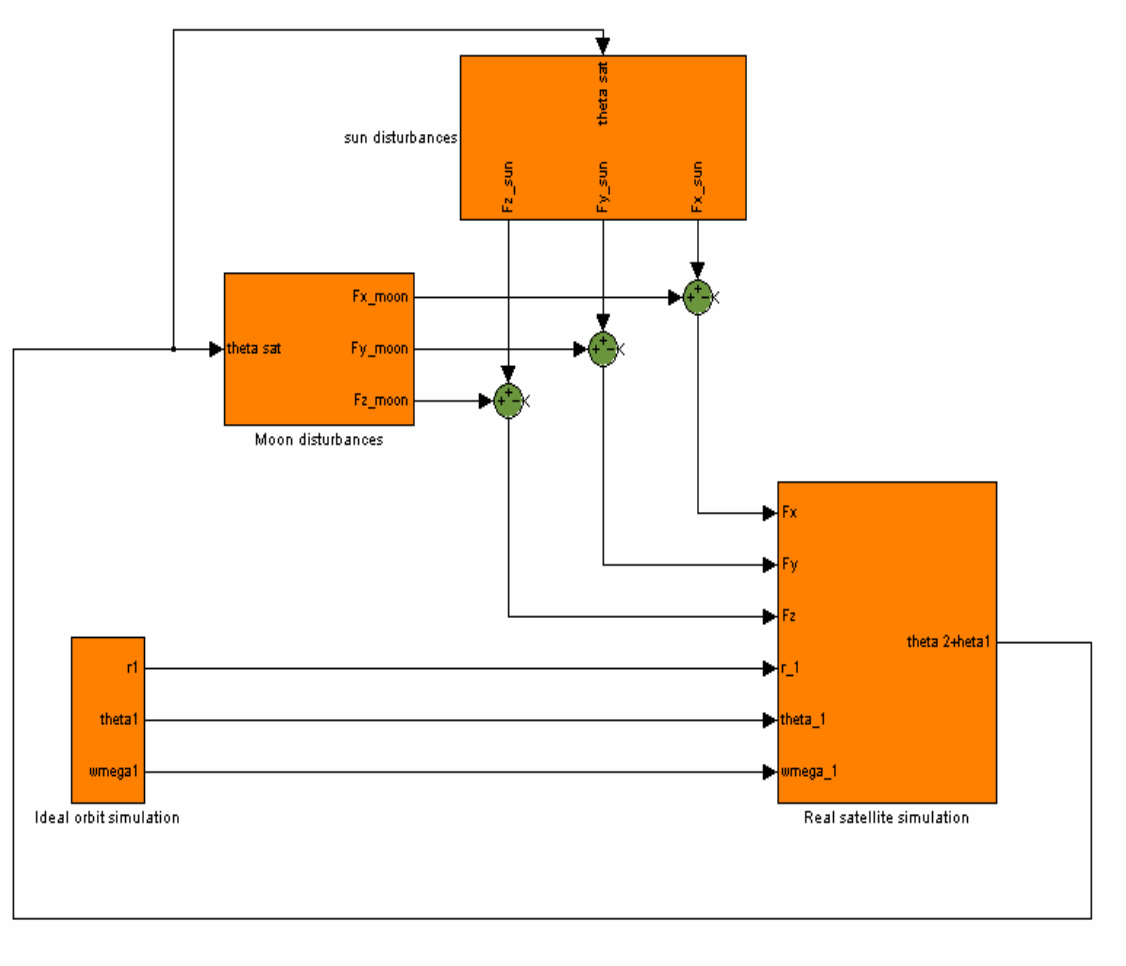

Figure 2.11.Simulink model of the equations of motion.

In Figure 2.12 a simulation result is shown, based on the above SIMULINK model, where the influence of all the perturbances acting on the satellite can be seen.

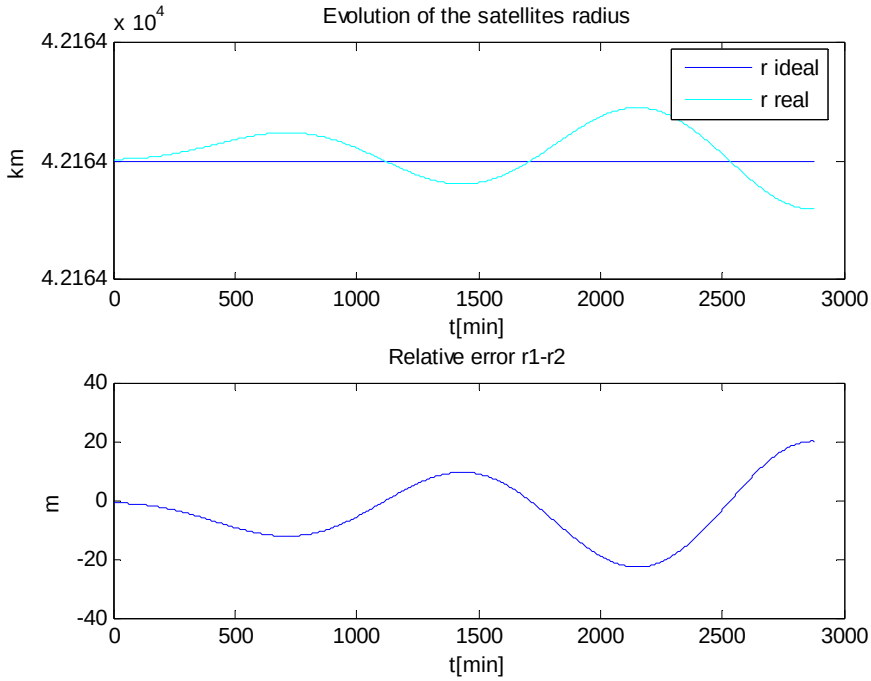

Figure 2.12.Evolution of the satellites radius as well as the relative error r1-r2 after the influence of all perturbances.

2.5. Thruster forces

In order to be able to control the satellite, there is a need of translatory acceleration to act on the body of the satellite. Those accelerations are provided mainly by the propulsion system.

Spacecraft propulsion systems are divided into three categories. Cold gas, chemicals (solid and liquid) and electrical, dependent on the way the trust is achieved. Propulsion systems, consists of several thrusters which their behavior is evaluated in terms of various characteristics. These basic characteristics include the thrust level F and the *specific impulse* I_{sp} described below.

The basic equation of propulsion holds for all kinds of propellants. The amount of thrust F can be calculated as:

$$F = V_e \frac{dm}{dt} + A[P_e - P_a] \qquad 2.27$$

where

P_e, P_a = gas and ambient pressures

V_e = exhaust velocity

A = area of the nozzle exit.

$\frac{dm}{dt}$ = mass flow rate of the propellant

The second parameter relevant to the characteristics of the thrust source is the *specific impulse* I_{sp} which is a measure of the efficiency with which the propellant mass is converted into thrust energy and is given by:

$$I_{sp} = F / \left(g \frac{dm}{dt} \right) \text{ measured in seconds.} \qquad 2.28$$

Besides the level of the thrust and the *specific impulse*, some additional characteristics are necessary in order to define a thruster completely, however this analysis is beyond the scope of this Thesis. For more information about propulsion systems and thrusters, the reader is directed to Sidi M. J. (1997).**Spacecraft Dynamics and Control** [1].

What is important for the purposes of testing the control methods that will be presented in detail in the next chapters is to define a limitation on the maximum absolute value of the force F that can be given by the thrusters. Usually for spacecraft control, liquid propeller thrusters are used which provide forces in the range of 0.001 – 100 N.

Chapter 3
Extended Kalman Filter

Symbols for Chapter 3:

$\hat{\mathbf{x}}$ = Estimated system states

e = Measurement noise.

υ = Process noise

u = System input

y = System output

Q = Process noise covariance matrix

R = Measurement noise covariance matrix

P = Estimate error covariance

L = Kalman gain to the predicted error $\mathbf{e}(t \mid t-1) = \mathbf{y}(t) - \hat{\mathbf{y}}(t \mid t-1)$,

Where, the notation (t|t-1) indicates the estimation at time t based on the information given to the state observer by time t-1

Chapters 3, 4, 5 and 6 are based on control theory, so in order to avoid confusion, a different and more specific notation is used in each Chapter.

3.1. Introduction.

The Kalman Filter (KF) was developed by Rudolf Kalman (1960) and it is basically a set of mathematical equations that provides an efficient computational (recursive) means to estimate the state of a process, in a way that minimizes the Mean Squared Error (MSE) between the real and estimated measurement.

Kalman filters are mainly used in applications where it is needed to provide updated information on a continuous basis about the states of a dynamic system when given only some measurements, corrupted by noise. Thus, it is essentially a state predictor that uses limited available information.

The Kalman filter addresses the general problem of trying to estimate the state $\hat{x} \in R^n$ (the caret ^ indicates the estimated states) of a discrete-time controlled process that is governed by the linear stochastic difference equation:

$$\mathbf{x}(t+1) = \mathbf{A}\mathbf{x}(t) + \mathbf{B}\mathbf{u}(t) + \boldsymbol{\upsilon}(t) \qquad 3.1$$

and the measurement output

$$\mathbf{y}(t) = \mathbf{C}\mathbf{x}(t) + \mathbf{D}\mathbf{u}(t) + \mathbf{e}(t) \qquad 3.2$$

where,
υ(t) and **e(t)** are the process and measurement noise.

In the case to be studied, these are assumed to be independent from each other (uncorrelated), white with zero mean, time uncorrelated and with normal probability distribution.

Then, the covariance $$\varepsilon\left\{\begin{bmatrix}\boldsymbol{\upsilon}(t)\\ \mathbf{e}(t)\end{bmatrix}\begin{bmatrix}\boldsymbol{\upsilon}(t)\\ \mathbf{e}(t)\end{bmatrix}^T\right\} = \begin{bmatrix}\mathbf{Q} & 0\\ 0 & \mathbf{R}\end{bmatrix}\delta\left(t_1 - t_2\right) \qquad 3.3$$

where, $\delta\left(t_1 - t_2\right) = \begin{cases} 1, & t_1 = t_2 \\ 0, \text{otherwise} \end{cases}$

Q and **R** are the process and measurement noise matrices.

In practice, the process noise covariance and measurement noise covariance matrices might change with each time-step or measurement. For the satellite problem however, it is assumed that they are constant.

The Kalman filter is a recursive estimator. This means that only the estimated state from the previous time step and the current measurement are needed to compute an estimate for the current state.

The state of the filter is represented by two variables:

- $\hat{\mathbf{x}}(t \mid t)$, the estimate of the state at time t
- $\mathbf{P}(t \mid t)$, the error covariance matrix (a measure of the estimated accuracy of the state estimate).

The Kalman filter can be described by two phases. The **Predict phase** and the **Update phase**.

In the predict phase, an estimation of the current state is made by using the information from the estimation of the previous timestep.

In the update phase, measurement information from the current timestep is used to refine this prediction to arrive at a new, more accurate estimate.

So, basically, what the Kalman state observer does, is to use the information of the system by including the dynamics of the system, and trying to minimize the error from the estimated to the real output. The error, $\mathbf{e}(t \mid t-1) = \mathbf{y}(t) - \hat{\mathbf{y}}(t \mid t-1)$ passes through the

Kalman gain L, which in the satellite case to be studied, it is time varying for more optimum estimations as shown in Figures 3.1 and 3.2 below.

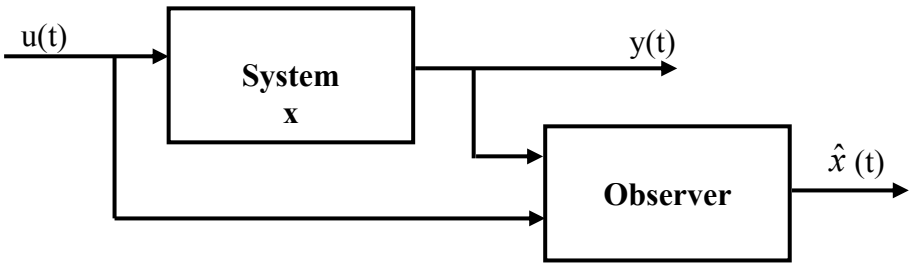

Figure 3.1.System with state observer.

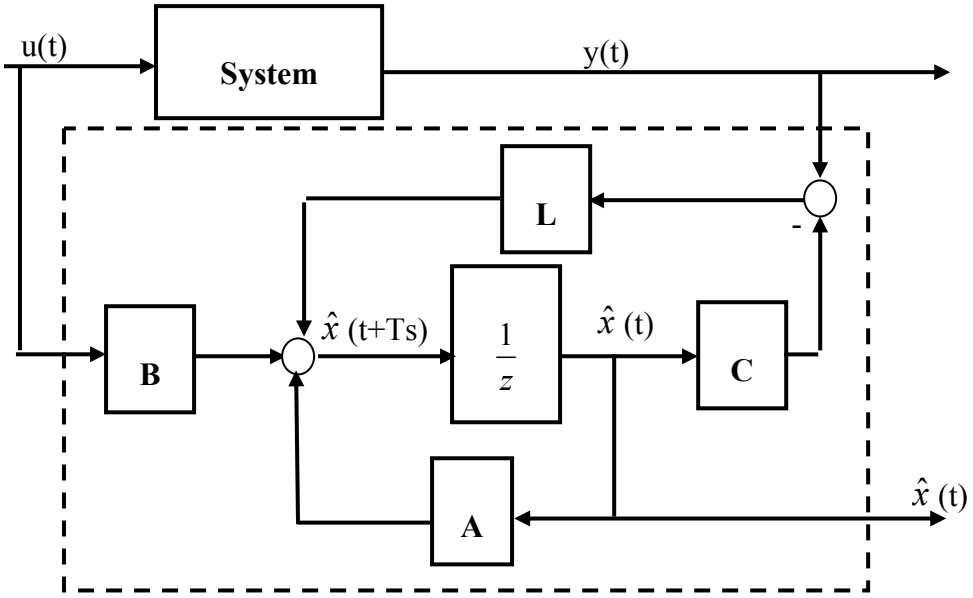

Figure 3.2.State observer.

As described above, the Kalman filter addresses the general problem of trying to estimate the state of a discrete-time controlled process that is governed by a linear stochastic difference equation.

However, in the case that the process to be estimated or the measurement relationship to the process is non-linear, a linearization must be done about the current mean and covariance and this is called the Extended Kalman Filter (EKF) which is the model that will be used for estimating the states of the satellite's system that is presented in this Thesis. The reason for that is because although the equations of motion are linear, what can be measured is non-linear.

3.2. The Extended Kalman Filer algorithm.

Let the system be described by:

$$\begin{aligned}\mathbf{x}(t+1) &= f(\mathbf{x}(t),\mathbf{u}(t),\boldsymbol{\upsilon}(t))\\ \mathbf{y}(t) &= g(\mathbf{x}(t),\mathbf{u}(t),\mathbf{e}(t))\end{aligned} \qquad 3.4$$

with $$\varepsilon\left\{\begin{bmatrix}\boldsymbol{\upsilon}(t)\\ \mathbf{e}(t)\end{bmatrix}\begin{bmatrix}\boldsymbol{\upsilon}(t)\\ \mathbf{e}(t)\end{bmatrix}^T\right\}=\begin{bmatrix}\mathbf{Q} & 0\\ 0 & \mathbf{R}\end{bmatrix}\delta\left(t_1-t_2\right)$$

Then,

$$\mathbf{y}(t) = g(\hat{\mathbf{x}}(t \mid t-1), \mathbf{u}(t), 0) + \mathbf{C}(t)(\hat{\mathbf{x}}(t) - \hat{\mathbf{x}}(t \mid t-1) + \boldsymbol{\Gamma}_{\mathbf{e}}(t)e(t) \qquad 3.5$$

where,

$\hat{\mathbf{x}}(t \mid t-1)$ indicates the estimation of the state $\hat{\mathbf{x}}$ at time *t* based on the information given to the state observer by time *t*-1

and **C***(t)* is the linearized **C** matrix in the case where the non-linearity is on the measurements, defined by:

$$\mathbf{C}(t) = \left.\frac{\partial g(\mathbf{x}, \mathbf{u}, \mathbf{e})}{\partial \mathbf{x}}\right|_{x=\hat{x}(t|t-1), u=u(t), e=0} \qquad 3.6$$

and

$$\boldsymbol{\Gamma}(t) = \left.\frac{\partial g(\mathbf{x}, \mathbf{u}, \mathbf{e})}{\partial \mathbf{e}}\right|_{x=\hat{x}(t|t-1), u=u(t), e=e(t)} \qquad 3.7$$

Then, the equations for the measurement update are:

$$\begin{aligned}
&\mathbf{L}(t) = \mathbf{P}(t \mid t-1)\mathbf{C}^{\mathbf{T}}(t)\left(\mathbf{C}(t)\mathbf{P}(t \mid t-1)\mathbf{C}^{\mathbf{T}}(t) + \boldsymbol{\Gamma}_{\mathbf{e}}(t)\mathbf{R}\boldsymbol{\Gamma}_{\mathbf{e}}{}^{\mathbf{T}}(t)\right)^{-1} \\
&\hat{\mathbf{x}}(t) = \hat{\mathbf{x}}(t \mid t-1) + \mathbf{L}(t)\{\mathbf{y}(t) - g(\hat{\mathbf{x}}(t \mid t-1), \mathbf{u}, 0\} \\
&\mathbf{P}(t \mid t) = \mathbf{P}(t \mid t-1) - \mathbf{L}(t)\left(\mathbf{C}(t)\mathbf{P}(t \mid t-1)\mathbf{C}^{\mathbf{T}}(t) + \boldsymbol{\Gamma}_{\mathbf{e}}(t)\mathbf{R}\boldsymbol{\Gamma}_{\mathbf{e}}{}^{\mathbf{T}}(t)\right)\mathbf{L}^{\mathbf{T}}(t)
\end{aligned} \qquad 3.8a.b.c$$

and for the time update are:

$$\begin{aligned}
&\hat{\mathbf{x}}(t+1, t) = f(\hat{\mathbf{x}}(t \mid t), \mathbf{u}(t), 0) \\
&\mathbf{P}(t+1 \mid t) = \mathbf{A}(t)\mathbf{P}(t \mid t)\mathbf{A}^{\mathbf{T}}(t) + \boldsymbol{\Gamma}_{\upsilon}(t)\mathbf{Q}\boldsymbol{\Gamma}_{\upsilon}{}^{\mathbf{T}}(t)
\end{aligned} \qquad 3.9.a.b$$

Where,

A*(t)* is the linearized **A** matrix in the case where the non-linearity is on the process to be estimated, defined by:

$$\mathbf{A}(t) = \left.\frac{\partial f(\mathbf{x},\mathbf{u},\boldsymbol{\upsilon})}{\partial \mathbf{x}}\right|_{x=\hat{x}(t|t),u=u(t),\upsilon=0} \qquad 3.10$$

and $\Gamma_u(t)$ is defined as:

$$\boldsymbol{\Gamma}_{\boldsymbol{\upsilon}}(t) = \left.\frac{\partial f(\mathbf{x},\mathbf{u},\boldsymbol{\upsilon})}{\partial \boldsymbol{\upsilon}}\right|_{x=\hat{x}(t|t),u=u(t),\upsilon=\upsilon(t)} \qquad 3.11$$

3.3 Application of the EKF to the satellite model.

As mentioned previously, in the case of estimating the satellite's states, an extended Kalman filter will be use, for the reason that the output measurements are non-linear.

The reason for that, is that basically what can be measured is the satellite's radius which is:

$$r_2 = \sqrt{(r_1 + x)^2 + y^2 + z^2} \qquad 3.12$$

where,

r_2 is the real satellite radius, r_1 is the ideal points radius, and x, y, z are the relative position coordinates of the satellite with respect to the ideal point.

The second and third measurements are again non-linear, which are $\dot{\mathbf{r}}_2$,and the latitude of the satellite, $\sin(lat) = \frac{z}{r_2}$

However, what is actually used in the algorithm for measurements, for making the calculations simpler but not having significant deterioration on the accuracy of the results, are:

$$\begin{aligned} y(1) &= r_2^2 - r_1^2 = 2r_1x + x^2 + y^2 + z^2 \\ y(2) &= \frac{1}{2}(r_2^{\,2}\dot{}) = (r_1 + x)\dot{x} + y\dot{y} + z\dot{z} \\ y(3) &= r_2 \sin(lat) = z \end{aligned} \qquad 3.13$$

3.3.1 State space equations in continuous and discrete time.

The equations of motion of the satellite, as presented in Chapter 2, are shown in 3.1.a, b and c below.

$$\begin{aligned} \ddot{x} &= 2nc\dot{y} + (5c^2 - 2)n^2x + f_x \\ \ddot{y} &= -2n\dot{x} + f_y \\ \ddot{z} &= -(3c^2 - 2)n^2z(t) + f_z \end{aligned} \qquad 3.14$$

where,

$$c = \sqrt{1 + \frac{3J_2\mu R_E^2}{8r_{ref}^{\,2}}(1 + 3\cos 2i_{ref})} \qquad 3.15$$

Then, the states of the system can be defined as:

$$\begin{bmatrix} x \\ \dot{x} \\ y \\ \dot{y} \\ z \\ \dot{z} \end{bmatrix} = \begin{bmatrix} x_1 \\ x_2 \\ x_3 \\ x_4 \\ x_5 \\ x_6 \end{bmatrix} \qquad 3.16$$

Finally, according to the equations of motion of 3.14.a.b.c, the state space equations can be calculated in continuous and discrete time, as shown henceforth.

Continuous time

$$\begin{aligned}
\dot{x}_1 &= x_2 \\
\dot{x}_2 &= 2ncx_4 + (5c^2 - 2)n^2 x_1 + f_x + \upsilon_x \\
\dot{x}_3 &= x_4 \\
\dot{x}_4 &= -2nx_2 + f_y + \upsilon_y \\
\dot{x}_5 &= x_6 \\
\dot{x}_6 &= -(3c^2 - 2)n^2 x_5 + f_z + \upsilon_z
\end{aligned} \qquad 3.17$$

and

$$y(t) = g(\mathbf{x}(t), \mathbf{u}(t), \mathbf{e}(t)) = \begin{bmatrix} 2r_1 x_1 + x_1^{\,2} + x_3^{\,2} + x_5^{\,2} + e_1 \\ (r_1 + x_1)x_2 + x_3 x_4 + x_5 x_6 \ + e_2 \\ x_5 + e_3 \end{bmatrix} \qquad 3.18$$

Discrete time

$$\begin{aligned}
x_1(t+1) &= x_1(t) + Tx_2(t) \\
x_2(t+1) &= 2Tncx_4(t) + T(5c^2 - 2)n^2 x_1(t) + x_2(t) + Tf_x + T\upsilon_x \\
x_3(t+1) &= x_3(t) + Tx_4(t) \\
x_4(t+1) &= -2Tnx_2(t) + x_4(t) + Tf_y + T\upsilon_y \\
x_5(t+1) &= x_5(t) + Tx_6(t) \\
x_6(t+1) &= -T(3c^2 - 2)n^2 x_5(t) + x_6(t) + Tf_z + T\upsilon_z
\end{aligned} \qquad 3.19$$

where,

T is the sampling time and the discretization was made by applying the derivative in T steps as shown below:

$$\dot{x}_1 = \frac{x_1(t+1) - x_1(t)}{T}$$

3.3.2 Calculation of A, B, C, D, Γ_e and Γ_u

For calculating the state space matrices in the extended Kalman filter, a linearization must be made around the area of the estimated values.

Then, for

$$\mathbf{x}(t+1) = f(\mathbf{x}(t), \mathbf{u}(t), \mathbf{\upsilon}(t))$$
$$\mathbf{y}(t) = g(\mathbf{x}(t), \mathbf{u}(t), \mathbf{e}(t))$$

the **A, B, C, D, Γ$_e$** and **Γ$_u$** matrices in discrete time are given by:

$$\mathbf{A} = \begin{bmatrix} 1 & T & 0 & 0 & 0 & 0 \\ T(5c^2-2)n^2 & 1 & 0 & 2Tnc & 0 & 0 \\ 0 & 0 & 1 & T & 0 & 0 \\ 0 & -2Tn & 0 & 1 & T & 0 \\ 0 & 0 & 0 & 0 & 1 & T \\ 0 & 0 & 0 & 0 & -T(3c^2-2)n^2 & 1 \end{bmatrix} \qquad 3.20$$

$$\mathbf{B} = \begin{bmatrix} 0 \\ 1 \\ 0 \\ 1 \\ 0 \\ 1 \end{bmatrix}, \mathbf{C}(t) = \begin{bmatrix} 2(\mathrm{r}_1 + x_1) & 0 & 2x_3 & 0 & 2x_5 & 0 \\ x_2 & \mathrm{r}_1 + x_1 & x_4 & x_3 & x_6 & x_5 \\ 0 & 0 & 0 & 0 & 1 & 0 \end{bmatrix} \qquad 3.21\ ,3.22$$

where,

$\mathbf{C}(t) = \left.\dfrac{\partial g(\mathbf{x},\mathbf{u},\mathbf{e})}{\partial \mathbf{x}}\right|_{x=\hat{x}(t|t-1),u=u(t),e=0}$ is the linearization of **C** matrix since the measured outputs are non-linear.

*g(***x, u, e***)* is given by 3.18

$$\mathbf{D}(t) = \begin{bmatrix} 0 & 0 & 0 \\ 0 & 0 & 0 \\ 0 & 0 & 0 \end{bmatrix} \qquad 3.23$$

And finally,

$$\mathbf{\Gamma_u} = \begin{bmatrix} 0 & 0 & 0 & 0 & 0 & 0 \\ 0 & T & 0 & 0 & 0 & 0 \\ 0 & 0 & 0 & 0 & 0 & 0 \\ 0 & 0 & 0 & T & 0 & 0 \\ 0 & 0 & 0 & 0 & 0 & 0 \\ 0 & 0 & 0 & 0 & 0 & T \end{bmatrix}, \quad \mathbf{\Gamma_e} = \begin{bmatrix} 1 & 0 & 0 \\ 0 & 1 & 0 \\ 0 & 0 & 1 \end{bmatrix} \qquad 3.24$$

3.4. Final results

The results of the extended Kalman filter will be presented in the following Figures, where a comparison of the real with the estimated states can be made.

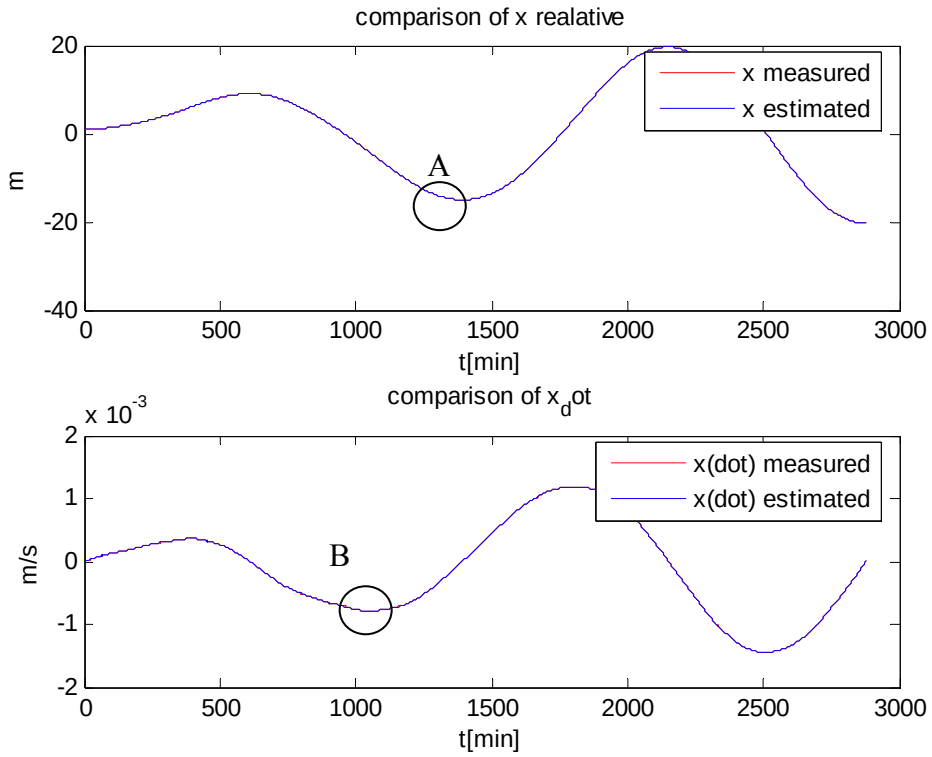

(a),(b)

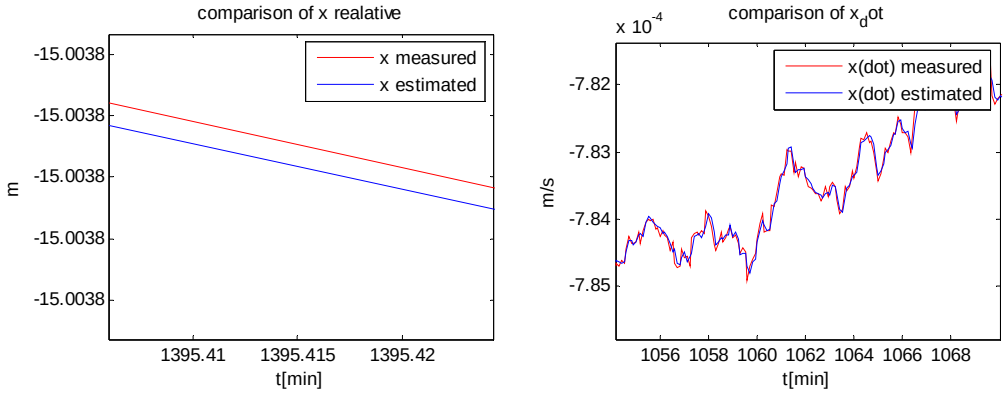

(c) (d)

Figure 3.3.Measured and estimated relative *x*.

a) *x* versus time. b) *x*(*dot*) versus time. c) Detail at region A, *x* versus time. d) Detail at region B, *x*(*dot*) versus time.

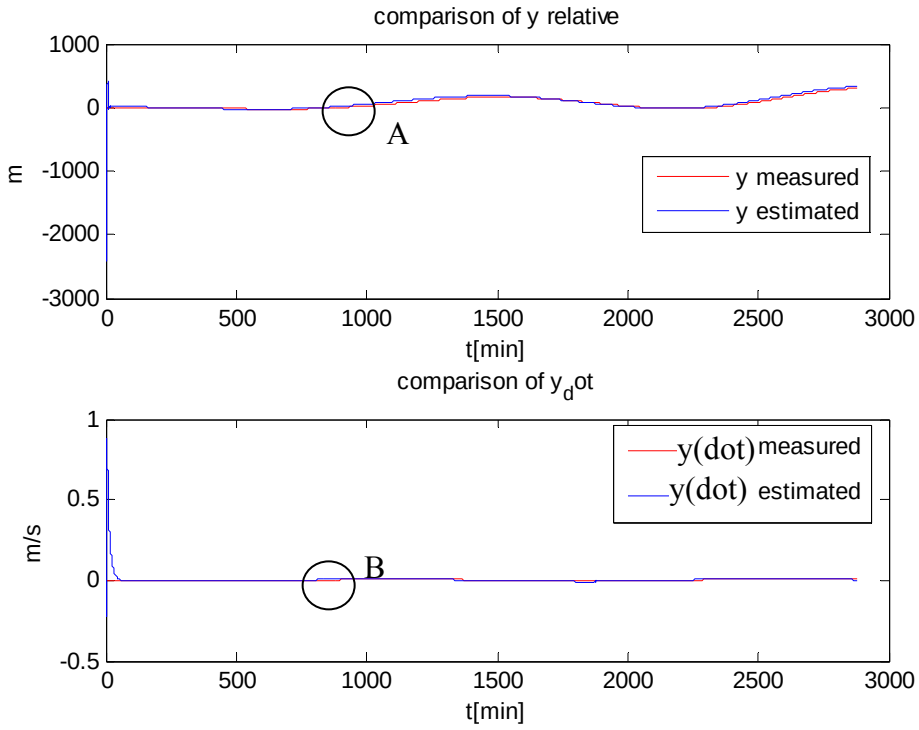

(a) ,(b)

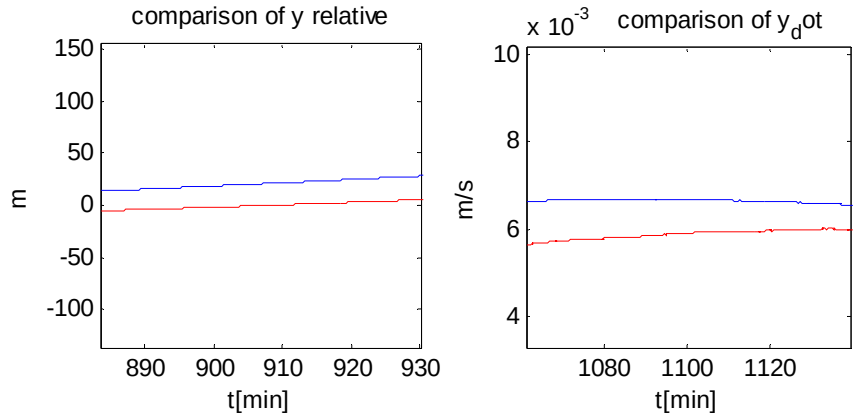

(c) (d)

Figure 3.4.Measured and estimated relative *y*.

a) *y* versus time.

b) *y*(*dot*) versus time.

c) Detail at region A, *y* versus time.

d) Detail at region B, *y*(*dot*) versus time.

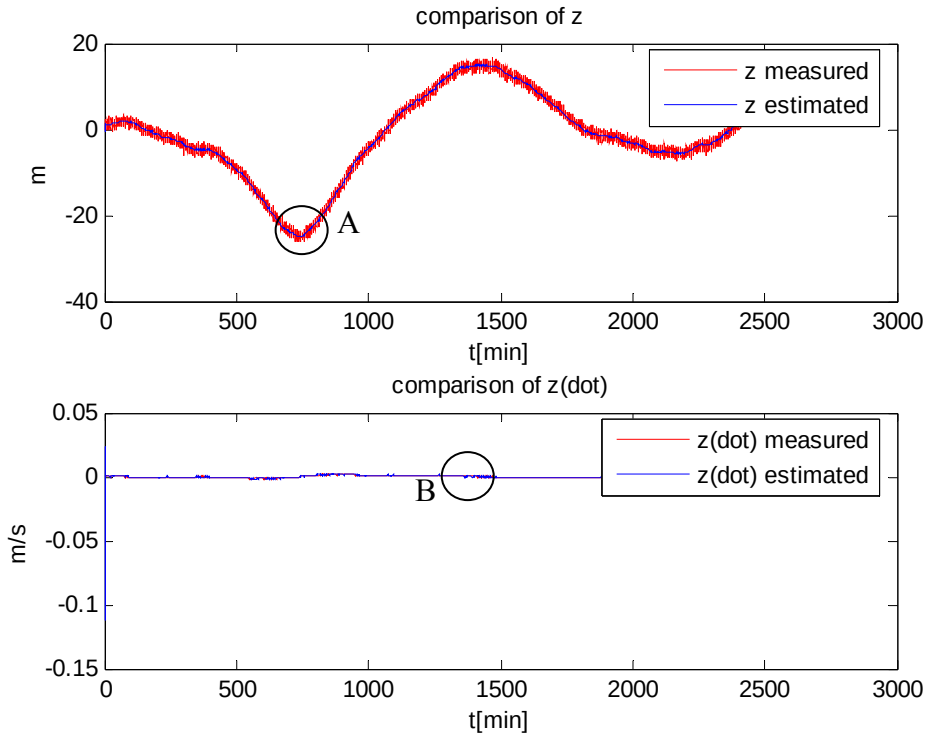

(a) and (b)

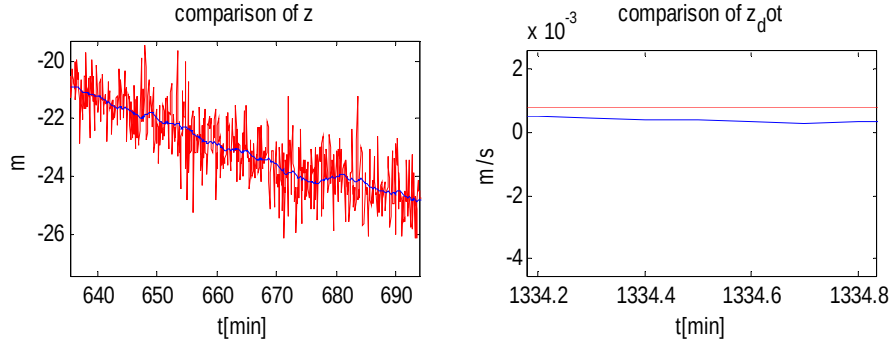

(c) (d)

Figure 3.5.Measured and estimated relative *z*.

a) *z* versus time.

b) *z*(*dot*) versus time.

c) Detail at region A, *z* versus time.

d) Detail at region B, *z*(*dot*) versus time.

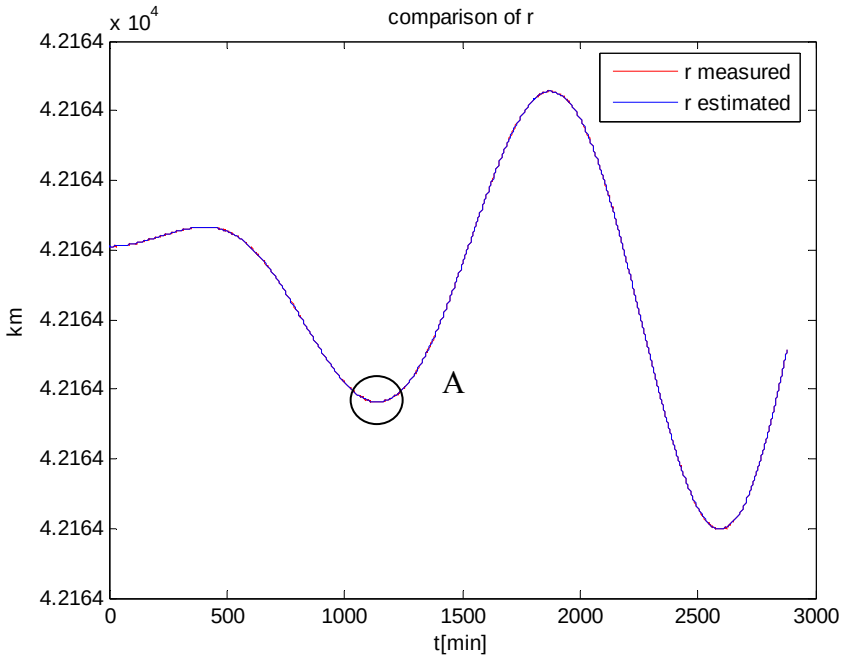

(a)

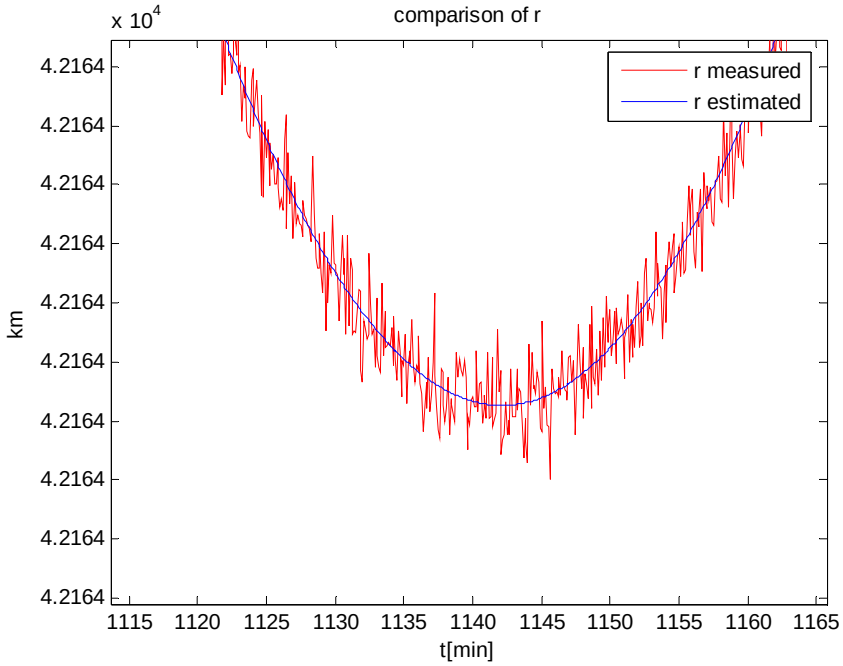

(b)

Figure 3.6.Measured and estimated r_2.

a) $\mathbf{r_2}$ versus time.

b) Detail at region A, $\mathbf{r_2}$ versus time.

Chapter 4
Linear Quadratic Regulator

Symbols for Chapter 4:

L = scalar performance index
u = control vector
λ = Lagrange multiplier
J = Performance index or cost function
Q, R, **S** = weighting matrices

4.1. Introduction.

In this chapter, a Linear Quadratic Regulator for discrete systems will be developed, which, basically, is a method of minimizing a cost function J associated with the control of a time varying system.

The analysis that follows is largely based on Lewis and Syrmos [6] approach, so the same notation as in the reference will be used.

A discrete time variant system could be described as

$$\mathbf{x}(t+1) = \mathbf{A}(t)\mathbf{x}(t) + \mathbf{B}(t)\mathbf{u}(t)\ ,\ \mathbf{x}(0) = \mathbf{x_0} \qquad 4.1$$

where the optimal control problem is to find the control $\mathbf{u}^*(t)$ that drives the system along a trajectory $\mathbf{x}^*(t)$ such that a suitable performance index or cost function (usually denoted by J) is minimized. The symbol * denotes the optimum variables.

An optimization analysis will first presented for a static system, when time is not a parameter, and then it will be extended to a system developing dynamically through time.

4.2. Static optimization.

Let $L(\mathbf{x}, \mathbf{u})$ be a scalar performance index, a function of the control vector $\mathbf{u} \in R^m$ and a state vector $\mathbf{x} \in R^n$. The problem is to select u to minimize $L(\mathbf{x}, \mathbf{u})$ and simultaneously satisfy the constraint given by equation $f(\mathbf{x}, \mathbf{u}) = 0$.

The Hamiltonian function is defined as:

$$H(\mathbf{x}, \mathbf{u}, \boldsymbol{\lambda}) = L(\mathbf{x}, \mathbf{u}) + \boldsymbol{\lambda}^{\mathrm{T}} f(\mathbf{x}, \mathbf{u}) \qquad 4.2$$

where,

$\boldsymbol{\lambda}$ is the set of the so-called Lagrange multipliers [6].

It is well known from advanced calculus that by equating independently to zero all derivatives of H, yields a stationary point.

In order then to have a minimum point of $L(\mathbf{x}, \mathbf{u})$ that also satisfies the constrain $f(\mathbf{x}, \mathbf{u}) = 0$ some conditions must be fulfilled.

Thus, the differential increments of H should be zero.

Increments in H, however, depend on increments in $\mathbf{x}$, $\mathbf{u}$ and $\boldsymbol{\lambda}$ according to:

$$dH = H_x^T dx + H_u^T du + H_\lambda^T d\lambda \qquad 4.3$$

The usefulness of the Lagrange multipliers approach can be mentioned at this point where in reality, dx and du are not independent increments. So, by introducing an undetermined multiplier $\boldsymbol{\lambda}$, we obtain an extra degree of freedom, and λ can be selected to make dx and du behave as if they were independent increments.

By introducing Lagrange multipliers we replace the problem of minimizing $L(\mathbf{x},\mathbf{u})$ subject to the constrain $f(\mathbf{x},\mathbf{u}) = 0$ with the problem of minimizing the Hamiltonian $H(\mathbf{x},\mathbf{u},\boldsymbol{\lambda})$.

Then the conditions for a minimum point of $L(\mathbf{x}, \mathbf{u})$ that also satisfy the condition $f(\mathbf{x}, \mathbf{u}) = 0$ are:

$$\frac{\delta H}{\delta \lambda} = f = 0$$
$$\frac{\delta H}{\delta x} = L_x + f_x^T \lambda = 0 \qquad \text{4.4 a, b, c}$$
$$\frac{\delta H}{\delta u} = L_u + f_u^T \lambda = 0$$

4.3. Optimal control of discrete-time systems.

The problem described previously can now be extended for a system that develops dynamically through time, since now the constraint equations are the dynamical equations describing the evolution in time of the system. These are governed and fixed by the basic physics of the system, through using fundamental laws and constitutive relations.

The performance index J (or cost function) that we seek to minimize is specified by us depending on the particular problem we seek to solve. Such a suitable J for the case of the satellite that has been studied is presented in the following sections.

4.3.1 Performance index *J* for the case of the satellite control problem

The general form of the performance index, is

$$J_i = \Phi(N, x_N) + \sum_{k=1}^{N-1} L_k(\mathbf{x_k}, \mathbf{u_k}) \qquad \text{4.5}$$

where,

[*i, N*] is the interval of interest in the behavior of the system.

$\Phi(N, \mathbf{x_N})$ is a function of the final time N and the state at the final time.

$L_k(\mathbf{x_k}, \mathbf{u_k})$ is a time varying function of the state and control input at each intermediate time L.

The optimal control then is to find the control $\mathbf{u}^*_k$ that drives the system along a trajectory $\mathbf{x}^*_k$ such that the performance index is minimized.

In the case of satellite orbit control, which is the objective of this Thesis work, it is desired to find an optimum control $\mathbf{u}^*_k$ that minimizes the energy needed to position the satellite both for the final and for the intermediate states.

Then, $J_i = \frac{1}{2}\mathbf{x}_N{}^T\mathbf{S}_N\mathbf{x}_N + \frac{1}{2}\sum_{k=1}^{N-1}(\mathbf{x}_k{}^T\mathbf{Q}_k\mathbf{x}_k + \mathbf{u}_k{}^T\mathbf{R}_k\mathbf{u}_k)$ 4.6

Where, **Q, R** and **S** are suitable weighting matrices.

Minimizing the energy corresponds to keeping the states and the control close to zero. Then, by proper weight matrices selection, an optimum control, in the sense of minimizing *J*, is found (calculated), which is the primary desired result.

For example if we want the intermediate states to be small, then **Q** should be chosen to be relatively large, so that it is heavily weighted in *J*. If the concern is that the control energy is small, then large values of **R** should also be selected.

In the case of the satellite's problem, it is desired to keep the intermediate states as small as possible. This means that the relative error is close to zero since the requirement is to take the satellite to the ideal orbit. However, this should be done with the minimum energy, so a trade-off between the weights **Q** and **R** should be made in order to achieve the optimum control.

4.3.2 Optimal Discrete-time Linear Quadratic Regulator.

The plant of the satellite that will be controlled is described by the linear equations below:

$\mathbf{x}(t+1) = \mathbf{A}(t)\mathbf{x}(t) + \mathbf{B}(t)\mathbf{u}(t)$, $\mathbf{x}(0) = \mathbf{x}_0$, 4.7

and the associated performance index is given by equation 4.6 were $\mathbf{Q_k}$, $\mathbf{R_k}$ and $\mathbf{S_k}$ are assumed to be symmetric positive semidefinite matrices and in addition $|\mathbf{R_k}| \neq 0$ for all k.

To solve this LQR problem, the following Hamiltonian function is used:

$$H_k = \frac{1}{2}(\mathbf{x_k}^T\mathbf{Q_k}\mathbf{x_k} + \mathbf{u_k}^T\mathbf{R_k}\mathbf{u_k}) + \boldsymbol{\lambda}_{k+1}^T(\mathbf{A_k}\mathbf{x_k} + \mathbf{B_k}\mathbf{u_k}) \quad 4.8$$

Then, the state and co-state equations are derived according to the Langrage multiplier formalism.

$$\mathbf{x_{k+1}} = \frac{\delta H_k}{\delta \boldsymbol{\lambda}_{k+1}} = \mathbf{A_k}\mathbf{x_k} + \mathbf{B_k}\mathbf{u_k} \quad \text{(State equation)} \quad 4.9$$

$$\boldsymbol{\lambda_k} = \frac{\delta H_k}{\delta \mathbf{x_k}} = \mathbf{Q_k}\mathbf{x_k} + \mathbf{A_k}^T\boldsymbol{\lambda}_{k+1} \quad \text{(Co-state equation)} \quad 4.10$$

and the stationary condition

$$0 = \frac{\delta H_k}{\delta \mathbf{u_\kappa}} = \mathbf{R_\kappa}\mathbf{u_\kappa} + \mathbf{B_\kappa}^T\boldsymbol{\lambda}_{\kappa+1} \quad 4.11$$

According to 4.11 then

$$\mathbf{u}_k = -\mathbf{R_k}^{-1}\mathbf{B_k}^T\boldsymbol{\lambda}_{k+1} \quad 4.12$$

Using equation 4.12 to eliminate $\mathbf{u_k}$ in 4.9, we get:

$$\mathbf{x_{k+1}} = \mathbf{A_k}\mathbf{x_k} - \mathbf{B_k}\mathbf{R_k}^{-1}\mathbf{B_k}^T\boldsymbol{\lambda}_{k+1} \quad 4.13$$

In the case of the control of the satellite's orbit, the final state $\mathbf{x_N}$ is free. This means that $\mathbf{x_N}$ can be varied while determining the constrained minimum, therefore, $d\boldsymbol{x_N} \neq 0$ and then it is required that [6]

$$\boldsymbol{\lambda_N} = \frac{d\Phi}{d\mathbf{x_N}} \quad 4.14$$

where Φ is the final state weighting function:

$$\Phi = \frac{1}{2}\mathbf{x_N}^T\,\mathrm{S_N}\,\mathbf{x_N} \quad 4.15$$

$$\Rightarrow \quad \boldsymbol{\lambda_N} = \mathrm{S_N}\,\mathbf{x_N} \quad 4.16$$

In order to solve these two boundary condition problems, the *sweep method* developed by Bryson and Ho (1975) is used.

That is to assume that a linear relation like 4.16 holds for all times $k \leq N$:

$$\Rightarrow \boldsymbol{\lambda}_{\mathbf{k}} = S_k \, \mathbf{x}_{\mathbf{k}} \qquad 4.17$$

For equation 4.17 to be valid, a consistent formula for S_k should exist.

So, by substituting 4.17 into 4.13 and solving for $\boldsymbol{x_{k+1}}$ we get:

$$\mathbf{x}_{\mathbf{k+1}} = (\mathbf{I} + \mathbf{B}_{\boldsymbol{\kappa}} \mathbf{R}_{\boldsymbol{\kappa}}^{-1} \mathbf{B}_{\boldsymbol{\kappa}}^{\mathrm{T}} S_{k+1})^{-1} \mathbf{A}_{\boldsymbol{\kappa}} \mathbf{x}_{\boldsymbol{\kappa}} \qquad 4.18$$

Then, if we substitute equation 4.17 to the co-state equation 4.10 and substitute $\boldsymbol{x_{k+1}}$ by 4.18, we have:

$$S_k \, \mathbf{x}_{\mathbf{k}} = \mathbf{Q}_{\mathbf{k}} \mathbf{x}_{\mathbf{k}} + \mathbf{A}_{\mathbf{k}}^{\mathbf{T}} S_{k+1} (\mathbf{I} + \mathbf{B}_{\boldsymbol{\kappa}} \mathbf{R}_{\boldsymbol{\kappa}}^{-1} \mathbf{B}_{\boldsymbol{\kappa}}^{\mathrm{T}} S_{k+1})^{-1} \mathbf{A}_{\boldsymbol{\kappa}} \mathbf{x}_{\boldsymbol{\kappa}} \qquad 4.19$$

Since $\mathbf{x_k}$ is generally non-zero, and equation 4.19 holds for all state sequences, then

$$S_k = \mathbf{A}_{\mathbf{k}}^{\mathbf{T}} S_{k+1} (\mathbf{I} + \mathbf{B}_{\boldsymbol{\kappa}} \mathbf{R}_{\boldsymbol{\kappa}}^{-1} \mathbf{B}_{\boldsymbol{\kappa}}^{\mathrm{T}} S_{k+1})^{-1} \mathbf{A}_{\boldsymbol{\kappa}} + \mathbf{Q}_{\mathbf{k}} \qquad 4.20$$

Finally by using the *matrix inversion lemma* [6] 4.20 become:

$$S_k = \mathbf{A}_{\mathbf{k}}^{\mathbf{T}} [S_{k+1} - S_{k+1} \mathbf{B}_{\boldsymbol{\kappa}} (\mathbf{B}_{\boldsymbol{\kappa}}^{\mathrm{T}} S_{k+1} \mathbf{B}_{\boldsymbol{\kappa}} + \mathbf{R}_{\boldsymbol{\kappa}})^{-1} \mathbf{B}_{\boldsymbol{\kappa}}^{\mathrm{T}} S_{k+1}] \mathbf{A}_{\boldsymbol{\kappa}} + \mathbf{Q}_{\mathbf{k}} \qquad 4.21$$

which is the well known *Riccati equation*.

If, however, $|\mathbf{S_k}| \neq 0$ for all k, then the *Riccati equation* can be rewritten as:

$$S_k = \mathbf{A}_{\mathbf{k}}^{\mathbf{T}} (S_{k+1}^{-1} + \mathbf{B}_{\boldsymbol{\kappa}} \mathbf{R}_{\boldsymbol{\kappa}}^{-1} \mathbf{B}_{\boldsymbol{\kappa}}^{\mathrm{T}})^{-1} \mathbf{A}_{\boldsymbol{\kappa}} + \mathbf{Q}_{\mathbf{k}} \qquad 4.22$$

Then the optimum control is given by:

$$\mathbf{u}_{\mathbf{k}} = -\mathbf{R}_{\boldsymbol{\kappa}}^{-1} \mathbf{B}_{\boldsymbol{\kappa}}^{\mathrm{T}} S_{k+1} \, \mathbf{x}_{\boldsymbol{\kappa+1}} \qquad 4.23$$

If again we substitute the plant equation 4.7 we finally get the optimum control by

$$\mathbf{u}_{\mathbf{k}} = -\mathbf{K}_{\boldsymbol{\kappa}} \mathbf{x}_{\mathbf{k}} \qquad 4.24$$

where $\mathbf{K_k} = (\mathbf{B_\kappa}^T S_{k+1} \mathbf{B_\kappa} + \mathbf{R_\kappa})^{-1} \mathbf{B_\kappa}^T S_{k+1} \mathbf{A_\kappa}$ 4.25

$\boldsymbol{K_k}$ is known as the Kalman gain

What is important to mention at this point is that the Kalman gain is given in terms of the *Riccati equation* solution S_k, the system and the weighting matrices. This means that it can be calculated off-line and then used on-line as shown in Figure 4.1 below.

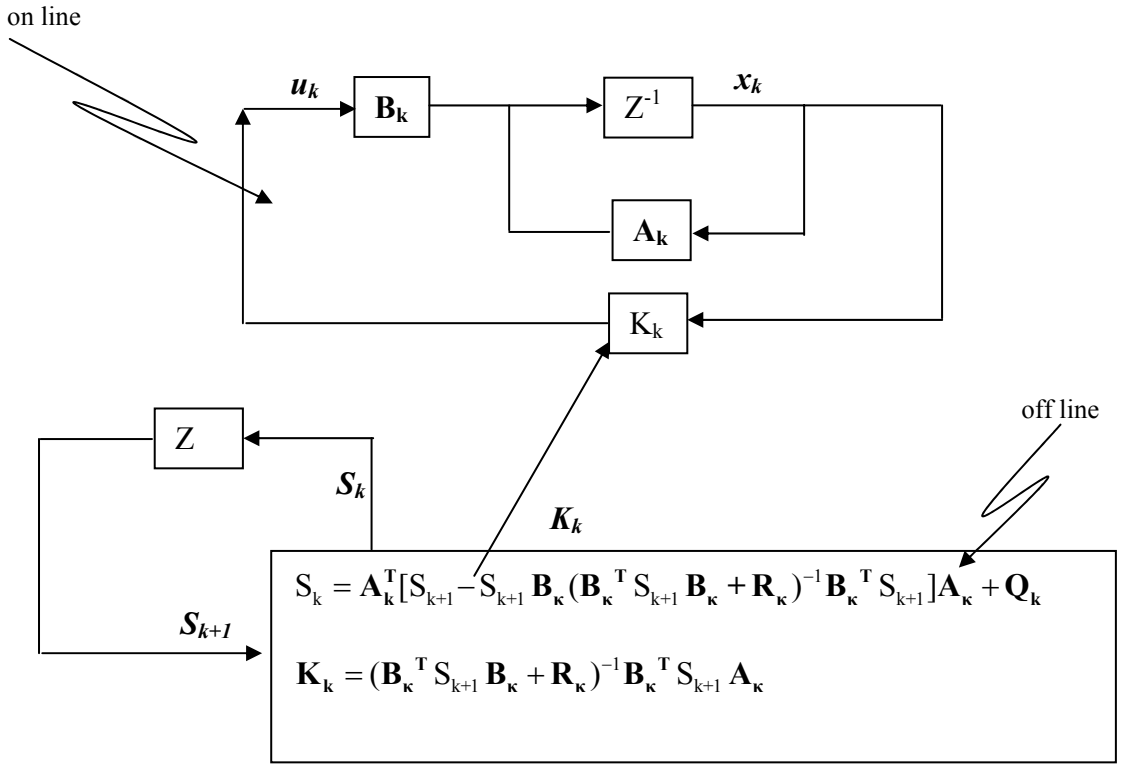

Figure 4.1.Free final state LQR optimal control scheme.

4.3.3 Steady-sate closed-loop control and suboptimal feedback

The closed-loop system described in the above section

$\mathbf{x_{k+1}} = (\mathbf{A_\kappa} - \mathbf{B_\kappa K_k})\mathbf{x_\kappa}$ 4.26

is time varying since the optimal feedback gains are time-varying.

However, this time-varying feedback is not always convenient to implement.
Instead, it is common to use a sub-optimal feedback gain

$$\mathbf{u_k} = -\mathbf{K}\mathbf{x_k} \qquad 4.27$$

which is easier to implement.
Basically, if the limit of the optimal $\mathbf{K_k}$ as the final time N goes to infinity exists, it provides a constant feedback which is often satisfactory.

The *Riccati equation* 4.21 is solved backward in time, beginning at time N.

Then, as $k \to -\infty$, the sequence S_k can have several types of behavior. It can converge to a steady-state matrix S_∞ which may be zero, positive semidefinite or positive definite. It may also fail to converge.

If, however, S_k does converge, then for large negative k, we have that

$$S \triangleq S_k \triangleq S_{k+1} \qquad 4.28$$

Thus, in the limit, the *Riccati equation* of 4.21 becomes:

$$S = \mathbf{A}^\mathbf{T}[S - S\mathbf{B}(\mathbf{B}^\mathbf{T}S\mathbf{B} + \mathbf{R})^{-1}\mathbf{B}^\mathbf{T}\mathbf{S}]\mathbf{A} + \mathbf{Q} \qquad 4.29$$

Which is the *Algebraic Riccati Equation* (ARE).

Then the limiting solution of 4.21 is of course also a solution of the ARE. However, since that ARE can also have non-positive semidefinite, nonsymmetric and even complex solutions, this means that not all the solutions of ARE are limiting solutions of the time-varying *Riccati equation.* If then the limiting solution of 4.21 exists and is denoted as S_∞, then the corresponding steady-state Kalman gain is:

$$\mathbf{K}_\infty = (\mathbf{B}^\mathbf{T}S_\infty\mathbf{B} + \mathbf{R})^{-1}\mathbf{B}^\mathbf{T}S_\infty\mathbf{A} \qquad 4.30$$

which is a constant gain.

What is important to know however, is when a limiting solution S_∞ exists and if the closed-loop plant is asymptotically stable.

The answer to these questions can be given by the following two theorems [6].

Theorem1:

Let **A, B** stabilizable, then for every choice of S_N there is a bounded limiting solution of S_∞. Furthermore, S_∞ is a positive semidefinite solution to the ARE. (for proof see [6])

Theorem2:

Let ***C*** be a square root of the intermediate state weighting matrix, so that

$\mathbf{Q} = \mathbf{C}^{\mathbf{T}}\mathbf{C} \geq 0$, and suppose that $\mathbf{R} > 0$. 4.31

If we suppose that (**A, C**) is observable, then (**A, B**) is stabilizable if and only if:

a) There is a unique positive definite limiting solution S_∞ to the *Ricccati equation* 4.21. Also S_∞ is the unique positive definite solution to the ARE.

b) The closed-loop plant

$$\mathbf{x}_{k+1} = (\mathbf{A}_\kappa - \mathbf{B}_\kappa \mathbf{K}_\infty)\mathbf{x}_\kappa \qquad 4.32$$

is asymptotically stable, where $\mathbf{K}_\infty$ is given by 4.30

What is basically stated by these two theorems is that if our system is stabilizable and if we select weighting matrix $\mathbf{Q} = \mathbf{C}^{\mathbf{T}}\mathbf{C}$ such as for some C the system is observable, then the steady-state feedback $\mathbf{u}_k = -\mathbf{K}_\infty \mathbf{x}_k$ is the optimal control, for it is the control that minimizes the performance criterion over the infinite time interval [0,∞].

4.4. Control of the satellite using LQ regulator - discrete system.

Following the above analysis, what has to be tested is the controllability and observability of the satellite's system.

Using the symbolic toolbox of MATLAB, it can be seen that the observability and controllability matrices have rank $n = 6$, which satisfies the criterion.

So, there exists a solution S_∞ which has been calculated with the MATLAB function

```
[S_inf, e, G] = dare(A, B, Q, R)
```

Finally the optimal control has been again found through the use of the MATLAB function:

```
[K1, S_inf, e] = dlqr(A, B, Q, R)
```

which internally calculates the discrete algebraic Riccati equation.

The selection of matrices **Q** and **R** was made based to the fact that the requirements are to have as little fuel energy utilization as possible.

For that case, matrix **R** and **Q** had been selected as

$$\mathbf{R} = \begin{bmatrix} 100 & 0 & 0 \\ 0 & 100 & 0 \\ 0 & 0 & 100 \end{bmatrix}, \qquad \mathbf{Q} = \begin{bmatrix} 1 & 0 & 0 & 0 & 0 & 0 \\ 0 & 1 & 0 & 0 & 0 & 0 \\ 0 & 0 & 1 & 0 & 0 & 0 \\ 0 & 0 & 0 & 1 & 0 & 0 \\ 0 & 0 & 0 & 0 & 1 & 0 \\ 0 & 0 & 0 & 0 & 0 & 1 \end{bmatrix} \tag{4.33}$$

The eigenvalues of the closed-loop system are:

```
e =
0.9156 + 0.0462i
0.9156 - 0.0462i
0.9161 + 0.0454i
0.9161 - 0.0454i
0.9159 + 0.0458i
0.9159 - 0.0458i
```

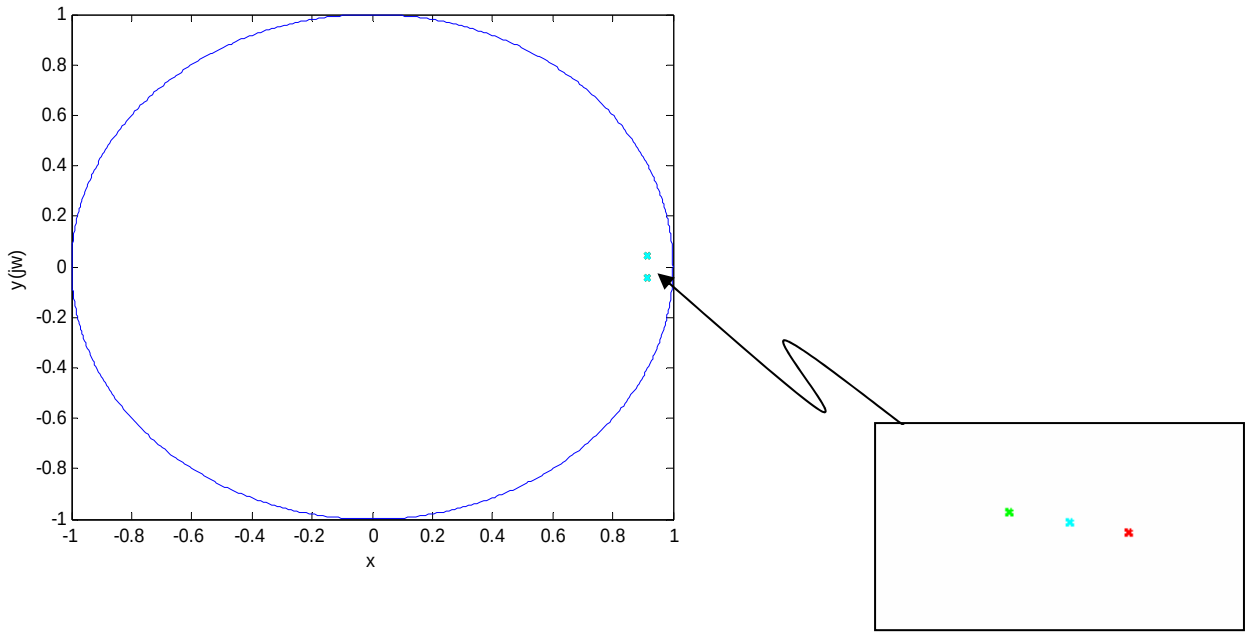

Figure 4.2.Eigenvalues of the closed-loop system.

As can be seen from Figure 4.2, the eigenvalue of the closed-loop system are within the stability margin.

4.5 Final results

In the following figures, the evolution of the states as well as the comparison of the real satellite with the ideal will be presented. The initial conditions of the satellite were:
$x = y = z =$ 1m. The time of the simulation was made to be 200 minutes, since after that period of time there is not significant difference in the satellites trajectory.

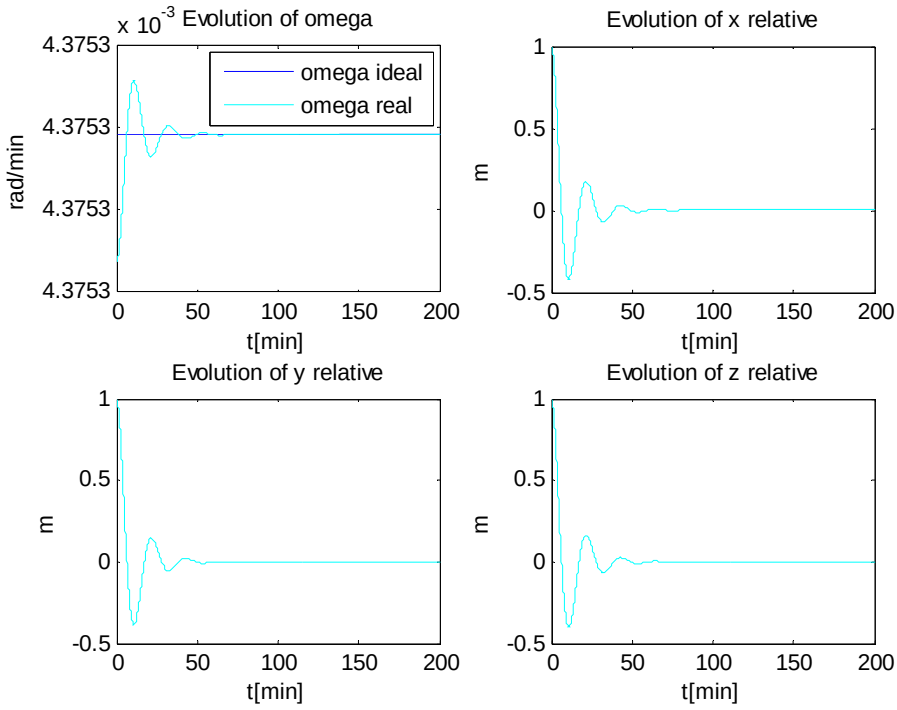

Figure 4.3.Measured and estimated states. a) angular velocity of the satellite (omega) versus time, b) *x* relative versus time, c) *y* relative versus time , d) *z* relative versus time

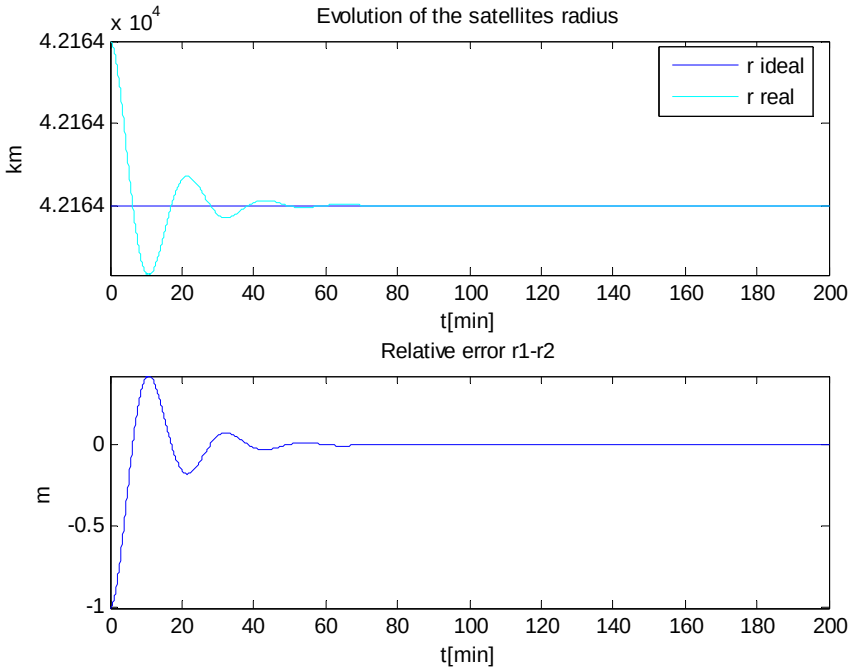

Figure 4.4.a.b Evolution of the satellites radius and the relative error.

Chapter 5
H-infinity Optimal Control Synthesis

Symbols for this Chapter:

G = plant model

G_d = disturbance model

$\boldsymbol{r}$ = reference input

$\boldsymbol{d}$ = disturbances

$\boldsymbol{y}$ = plant outputs

y_m = measured $\boldsymbol{y}$

$\boldsymbol{u}$ = control signals

P = generalized plant includes G and G_d and the interconnection structure between the plant and the controller.

$\boldsymbol{w}$ = exogenous inputs (commands, disturbances, noise)

$\boldsymbol{z}$ = exogenous outputs

$\boldsymbol{v}$ = controller inputs for the general configuration (measured signals)

L = GK loop transfer function (K = controller transfer function)

S = $(1+L)^{-1}$ sensitivity function

T = $((1+L)^{-1} L)$ complementary sensitivity function

DEFINITIONS:

Maximum peaks:

$$M_s \equiv \max_{\omega} |S(j\omega)|$$

and

$$M_T \equiv \max_{\omega} |T(j\omega)|$$

Typically, $M_s \leq 2$ and $M_T < 1.4$

Bandwidth:

Bandwidth is defined as the frequency range $[\omega_1, \omega_2]$ over which control can be affective. Usually, but not always, $\omega_1 = 0$ and $\omega_2 \equiv \omega_B$ is the bandwidth.

The closed-loop bandwidth is the frequency where $|S(j\omega)|$ first crosses the magnitude ratio of $1/\sqrt{2} = 0.707 \simeq -3dB$ from below, while the bandwidth in terms of T, ω_{BT} is the highest frequency where $|T(j\omega)|$ crosses $1/\sqrt{2} = 0.707 \simeq -3dB$ from above.

ω_C ≡ cross over frequency, which is the frequency where $|L(j\omega)|$ first crosses a magnitude ratio of 1 from above.

5.1. H_∞ controller synthesis

The main task of the problem is to design a controller that can stabilize the satellite and control its trajectory, irrespective of external influences which are mainly disturbances caused by the sun's and moon's gravitational field as well as from the non-homogeneity and oblateness of the earth.

The approach that will be developed, demonstrated, simulated and appraised in this chapter is the so-called H_∞ controller ("*H*" stands for Hardy spaces, while the infinity subscript indicates a minimax optimization). The H_∞ controller is essentially an optimal controller that can be applied to MIMO systems .This controller will be described in some detail below.

A deterministic MIMO system can be represented by the following block diagram, (Figure 5.1)

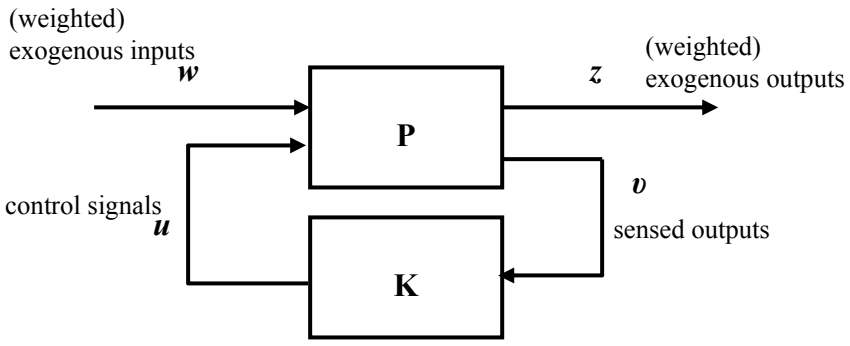

Figure 5.1.General control configuration with no uncertainty.

The overall control objective is to find a controller *K*, which, based on the information in **υ**,to generate control signals **u** that will counteracts the unwanted influence of **w** on **z**. by minimizing some suitable norm (in this case the H_∞ norm) of the transfer function relating **w** to **z.**

That is, in the case of the control of the satellite's orbit, to find a controller that counteracts the external disturbances acting on the satellite by minimizing the closed-loop norm from **w** to **z**.

The H_∞ norm of a scalar transfer function *f(s)* is simply the peak value of $|f(j\omega)|$ as a function of frequency.
That is,

$$\|f(s)\|_\infty \triangleq \max_\omega |f(j\omega)| \qquad 5.1$$

The H_∞ controller synthesis is basically a design method that tries to press down the peaks of one or selected transfer functions. The ∞ symbol, comes from the fact that the maximum magnitude over frequency can be written as

$$\max_\omega |f(j\omega)| = \lim_{p\to\infty}\left(\int_{-\infty}^{\infty} |f(j\omega)|^p \, d\omega\right)^{1/p} \qquad 5.2$$

That can be translated as taking the peak value of $|f|$ by raising it at infinite power, since $p \to \infty$.
So, with this definition, H_∞ is the set of transfer functions with bounded ∞-norms [11].

5.1.1 Scaling.

In the analysis that follows, in order to simplify the controller design and the performance analysis, the inputs, outputs and disturbances of the system are normalized by suitable scaling of the general transfer function *G*.

For MIMO systems, such as the case to be studied, in order to scale the inputs and outputs of the system, the unscaled variables are divided by the maximum expected or allowed value.

If $\mathbf{D_d}$, $\mathbf{D_u}$, and $\mathbf{D_e}$ define the diagonal scaling matrices for the disturbances, inputs and error (output), then the scaled variables are obtained by:

$$\mathbf{d} = \mathbf{D_d}^{-1}\hat{y}\ ,\ \mathbf{u} = \mathbf{D_u}^{-1}\hat{u} \quad \text{and} \quad \mathbf{y} = \mathbf{D_e}^{-1}\hat{y} \tag{5.3}$$

where the caret ^ indicates scaled variables.

Similarly, the scaled transfer functions will be:

$$G = \mathbf{D_e}^{-1}\hat{G}\mathbf{D_u} \text{ and } G_d = \mathbf{D_e}^{-1}\hat{G}_d\mathbf{D_d} \tag{5.4}$$

where G is the satellite's model transfer function and G_d the disturbances transfer function. Since however, for the case of the satellite the disturbances are inertial forces expressed as accelerations acting on the mass of the satellite, then the disturbances can be considered as external forces acting on the plants input, so $G_d = G$.

5.2. Controller design

There are mainly three approaches to the controller design.

a) By proper shaping of the open and closed-loop transfer functions.
b) By the so-called signal-based approach, which this basically considers a disturbance or reference change and tries to optimize the closed loop response (LQG control).
c) A numerical optimization: Multi-objective optimization to optimize directly the true objectives such as rise time and stability margins.

The H_∞ controller synthesis is based on the first approach, where the amplitude of the open-loop transfer function $L(j\omega)$ is shaped, as well as the closed-loop transfer functions S, T and KS.

5.2.1. Open- loop shaping

By shaping the open-loop transfer function $L(j\omega)$, some fundamental trade-offs must be taken, such as:

1. For good disturbance rejection, L must be large.
2. For a good command following (small errors), L must be large.
3. For measurement noise reduction, L must be small.
4. To keep the magnitude of the input signals small, K must be small and L must be small.

The specifications of the desired loop transfer function are:

1. The gain crossover frequency ω_c where $L(j\omega) = 1$
2. The slope N of $|L(j\omega)|$ in certain frequency ranges, where typically the slope

N=(-20dB/dec) around the crossover and a larger roll-off at higher frequencies. The desired slope at low frequencies depends on the nature of the reference signal or of the disturbances.

As mentioned before, in the case of the satellite's control, it is of primary interest to achieve good disturbance rejection.

5.2.2 Loop shaping for disturbance rejection

The basic control problem can be described as

$\mathbf{y} = G_u\mathbf{u} + G_d\mathbf{d}$

and the regulator problem is to counteract the disturbances **d**.

That is the goal of the control is to make

$\mathbf{e} = \mathbf{y} = SG_d\mathbf{d}$ minimum.

So, for achieving $|e(j\omega)| \leq 1$ for $|d(j\omega)| = 1$ (which is the worst case), then

$$\left|SG_d(j\omega)\right| \leq 1 \quad \text{or} \quad \left|1+L\right| \geq \left|G_d\right| \quad \forall\omega \qquad 5.5$$

Or, approximately

$$|L| \geq |G_d| \ \forall \omega$$

So one good initial guess would be that

$$|L|_{\min} \approx |G_d| \ \forall \omega$$

Finally, at this point it may be concluded that the controller should contain the dynamics of the disturbance (G_d) and invert the dynamics of the inputs (G)

For disturbances at the plant output G_d =1 while for the case that will be examined where the disturbances are at the plants input, $G_d = G$

More specifically, the loop shape *L(s)* for our case could be modified based on the three points below:

1. Around crossover the slope to be around -1 for transient behavior with acceptable gain and phase margins
2. The loop gain should be increased for improving the settling time and reduce the steady state offset.
3. *L(s)* should also roll off faster at higher frequencies beyond the bandwidth in order to reduce the use of manipulated inputs and make the controller realizable. Also for noise reduction.

5.2.3 Closed-loop shaping

For closed-loop shaping, we are interested in *S* and *T*.

In the high frequencies where $|L(j\omega)| >> 1$ then,
$S \approx L^{-1}$ and $T \approx 1$,
while in the lower frequencies where $|L(j\omega)| << 1$
$T \approx L^{-1}$ and $S \approx 1$

However, in the crossover region where $|L(j\omega)| \approx 1$, nothing can be inferred about S and T.

The sensitivity function S is a good indicator of a closed-loop performance, both for SISO and MIMO systems. Ideally, S must be small.

Typical specifications in terms of S include:

1. Minimum Bandwidth ω_B
2. Maximum tracking error at selected frequencies
3. The maximum steady state tracking error A
4. Shape of S over selected frequency ranges
5. Maximum peak magnitude of S, $\|S(j\omega)\|_\infty \le M_s$

The typical values of M_s =2. Peak specifications prevent amplification at high frequencies, as well as introduce a margin of robustness.

These specifications may be captured by an upper boundary, $1/|\mathbf{w}_P(s)|$ on S, where $\mathbf{w_P}$ is the performance weight and is mainly used as a performance indicator.

Then the performance requirements, become:

$$|S(j\omega)| < \frac{1}{|\mathbf{w}_P(j\omega)|} \qquad \forall\omega \tag{5.6}$$

$$\Rightarrow \quad \|\mathbf{w}_P(S)\|_\infty < 1$$

The typical performance weight, is:

$$\mathbf{w}_p(s) = \frac{\frac{s}{M_s} + \omega_B}{s + \omega_B A}, \tag{5.7}$$

What is of our interest is that

$$|S(j\omega)| < \frac{1}{|\mathbf{w}_P(j\omega)|} \ \forall\omega, \tag{5.8}$$

$$\Rightarrow |S(j\omega)| < 1/|\mathbf{w}_P(j\omega)| \forall\omega$$

so, what can be seen here is that at low frequencies, the weighting filter $1/|\mathbf{w}_P|$ is equal to A.

So, typically A should be very close to zero in order to ensure approximate integral action with $S(0) \approx 0$. However, for avoiding calculation errors, A usually takes a very small value.

The desired closed-loop bandwidth ω_B may be different for each output of the filter weight and depends on the position of the zeros of the system. A large value of ω_{Bi} yields a faster response for output *i.*

Also, an additional upper boundary can be added for the magnitude of T in order to make sure that L does not roll off fast at high frequencies as well as to achieve robustness.

That can be done by setting

$$\left|T(j\omega)\right| < \frac{1}{\left|\mathbf{w}_T(j\omega)\right|} \quad \forall \omega, \tag{5.9}$$

where $\mathbf{w_T}$ is known as the weight for robustness.

To restrict the magnitude of the input signals $\mathbf{u} = -KSG_d\mathbf{d}$ an upper bound on the magnitude of KS can be placed. That is to be less than $1/|\mathbf{w_u}|$ where $\mathbf{w_u}$ is the input weight.

By combining these mixed sensitivity specifications the following "stacking approach" results.

$$\left\|N\right\|_\infty = \max_\omega \bar{\sigma}\left|N(j\omega)\right| < 1 \tag{5.10}$$

where $N = \begin{bmatrix} \mathbf{w}_u KS \\ \mathbf{w}_T T \\ \mathbf{w}_P S \end{bmatrix}$ and $\bar{\sigma}$ denotes the maximum singular value.

The optimal controller is then obtained by solving the problem

$$\min_K \left\|N(K)\right\|_\infty$$

Numerically this problem is solved by the so-called γ-iteration where the solution is for a controller that achieves $\left\|N\right\|_\infty < \gamma$. Then γ is reduced iteratively to obtain the smallest value of γ for which solution exists.

5.3. Limitations on performance.

5.3.1 Limitations on sensitivity.

From the definitions of S and T, it can be derived that

$$S+T=\mathrm{I} \qquad 5.11$$

Ideally, S should be small to obtain small control error for the disturbances as well as small T to avoid sensitivity to noise. Unfortunately, these requirements are not simultaneously possible since at any frequency, either $|S(j\omega)|$ or $|T(j\omega)|$ must be larger or equal to 0.5.

However, for MIMO systems, which is the case that will be examined, from eq. 5.11 it can be seen that:

$$\left|\bar{\sigma}(S)-1\right| \le \bar{\sigma}(T) \le \bar{\sigma}(S)+1 \qquad 5.12a$$

and

$$\left|\bar{\sigma}(T)-1\right| \le \bar{\sigma}(S) \le \bar{\sigma}(T)+1 \qquad 5.12b$$

These can be combined to get

$$\left|\bar{\sigma}(S)-\bar{\sigma}(T)\right| \le 1 \qquad 5.12c$$

So, it is only possible for the magnitudes of $\bar{\sigma}(S)$ and $\bar{\sigma}(T)$ to differ by at most 1 at a given frequency.

There is also a limitation due to *interpolation constrains*, where if p is a RHP pole of the plant $G(s)$, then $T(p) = 1$ and $S(p) = 0$. Similarly, if z is a RHP zero of $G(s)$ then $T(z) = 0$ and $S(z) = 1$.

The main difference for MIMO systems is that basically for a multivariable system, the plant gain, RHP poles and zeros as well as disturbances, all have directions associated

with them. Poles and zeros directions, which is of primary concern, may be obtained from a singular value decomposition (SVD) of *G(p)* or *G(z)* [11]

So, basically for MIMO systems, from interpolation constrains, if *G(s)* has a RHP zero at *z* with output direction y_z then for internal stability of the feedback system, *T* must have a RHP pole in the same direction as *G* and that *S(z)* has an eigenvalue of 1 corresponding to the left eigenvector y_z.
That is,
$y_z^H T(z) = 0$ and $y_z^H S(z) = y_z^H$, where y^H is the conjugate transpose.

If *G(s)* has a RHP pole at *p* with output direction y_p then for internal stability
$S(p)y_p = 0$ and $T(p)y_p = y_p$

One other limitation on sensitivity is what is known as the *waterbed effect* that basically states that if we push the sensitivity down at some frequencies, then it will have to increase at others.

In general, a trade-off between sensitivity reduction and sensitivity increase must be performed whenever *L(s)* has at least two more poles than zeros or *L(s)* has a right hand plane (RHP) zero.

5.3.2 Limitations on peaks

The term 'peak' at this point means the maximum value of the frequency response or the H_∞ norm of important transfer functions such as *S* and *T*. So the main concern is to derive explicit bounds on these transfer functions.

From the *Maximum modulus principle* [11], which basically states that for a stable *f(s)* , then the maximum value of |*f(s)*| (for *s* in the right-hand plane) is attained on the region's boundary.
More specifically,

$$\left\| f(j\omega) \right\|_\infty = \max_\omega \left| f(j\omega) \right| \geq \left| f(s_0) \right| \qquad \forall \quad s_0 \in \text{RHP} \qquad 5.13$$

Then by considering that $|f(s)| = \mathbf{w}_p(s)S(s)$ and $|f(s)| = w_T(s)T(s)$

the following theorems are true.

Weighted sensitivity theorem:

If *G(s)* has a RHP zero *z* and $\mathbf{w}_p$ is any stable weight, then for closed-loop stability, the weighted sensitivity function must satisfy

$$\|\mathbf{w}_p S\|_\infty \geq \mathbf{w}_p(z) \qquad 5.14a$$

For MIMO systems,

$$\|\mathbf{w}_p(s)S(s)\|_\infty = \max_\omega \bar{\sigma}(\mathbf{w}_p(j\omega)S(j\omega)) \geq |\mathbf{w}_p(z)| \qquad 5.14b$$

In MIMO systems, we generally have the freedom to move the effect of RHP zeros to different outputs by appropriate control.

Weighted complementary sensitivity theorem:

If *G(s)* has a RHP pole *p* and $\mathbf{w}_T$ is any stable weight, then for closed-loop stability, the weighted sensitivity function must satisfy

$$\|\mathbf{w}_T T\|_\infty \geq \mathbf{w}_T(p) \qquad 5.15a$$

The above theorem for MIMO systems becomes:

$$\|\mathbf{w}_p(s)S(s)\|_\infty = \max_\omega \bar{\sigma}(\mathbf{w}_p(j\omega)S(j\omega)) \geq |\mathbf{w}_p(z)| \qquad 5.15b$$

Also the weighted sensitivity and complementary sensitivity have limitations on their peaks caused by combination of RHP poles and zeros as well as from pairs of complex poles and zeros. All the above constrains have as effect the limitations on the bandwidth ω_B, which is a major factor on the selection of the weighting filters.

However, since for the case of the satellite's model that is studied, it is of primary concern the rejection of disturbances, the following analysis is about bandwidth limitation on low frequencies.

5.3.3 Bandwidth limitation

5.3.3.1 RHP-zero and performance at low frequencies

By considering the performance weight $\mathbf{w}_p(s) = \frac{s/M_s + \omega_B}{s + \omega_B A}$, a minimum bandwidth ω_B is defined by the performance limitation: $|S(j\omega)| < 1/|\mathbf{w}_P(j\omega)|, \ \forall\omega$.

Also maximum peak of |S| less than M_s and a steady-state offset less than A<1. If then the plant has a RHP-zero at $s=z$ then from 5.14 a we have that

$$|\mathbf{w}_p(z)| = \left|\frac{z/M_s + \omega_B}{z + \omega_B A}\right| < 1 \qquad 5.16$$

In the case that z is real then all variables are real and positive and from 5.16 we derive the bound on ω_B.

$$\Rightarrow \omega_B < z\frac{1 - 1/M_s}{1 - A} \qquad 5.17$$

If we assume A=0 and M_s=2 we must at least have that $\omega_B < 0.5z$

In the case that the system has a pair of complex conjugate RHP- zeros,
$z = x \pm jy, \ x \geq 0$, A=0 and M_s=2 then:

$$\omega_B < -0.5x + \sqrt{x^2 + 0.75y^2}$$

5.3.3.2 Limitations imposed by unstable (RHP) poles.

By making similar assumptions as above, that is A=0 and M_T =2 and considering as a complimentary sensitivity weight

$$\mathbf{w}_T(s) = \frac{s}{\omega_{BT}} + \frac{1}{M_T} \qquad 5.18$$

Then for a real RHP-pole at $s = p$ and from the robustness limitation

$|T(j\omega)| < 1/|\mathbf{w}_T(j\omega)|, \quad \forall\omega$, Results that the minimum $\omega_B > 2p$

Similarly, for a pair of complex RHP poles $p = x \pm jy, \ x \geq 0$ then:

$$\omega_B > 0.67(x + \sqrt{4x^2 + 3y^2}) \qquad 5.19$$

The above approximations are made for SISO systems. In the case of MIMO systems, lower bounds on various closed-loop functions can be derived by direct generalizations of those from the SISO systems if only the directions are taken into account.

In the case of the satellite's MIMO model, G_{sat} has the following poles and zeros which they were derived by the MATLAB function `tzero(G)` and `pole(G)`

Poles:	0 0.0000 + 0.0044i 0.0000 - 0.0044i 0 0.0000 + 0.0044i 0.0000 - 0.0044i	Zeros:	20.0000 + 0.0000i 20.0000 - 0.0000i 20.0000 20.0000 20.0000 20.0000

By observing the poles and zeros of the system, what can be inferred to at this point is that $\omega_B < 10\ rad/\mathrm{s}$. The second observation is that the system has six poles on the imaginary axis. This can cause a calculation problem when the MATLAB function `hinfopt` is called to calculate the optimum controller. However, this issue will be analyzed in the last part of this chapter.

5.3.4 Functional controllability

In order to be able to control all outputs independently, it is required that the normal rank of the plant $G_{sat}(s)$ has the same rank as the number of outputs. This is basically the definition of functional controllability, where in the case of the satellite's model, if we define n the normal rank of G_{sat} then it can be seen that $n = 3$ which is the number of the system's outputs. This means that the satellite's system is functionally controllable.

All of the above analysis however, is a good indicator for the selection of the initial filter weights. What follows next is a lot of simulations and with trial and error the optimum controller is selected.

5.4. The general control problem.

As described in the introduction of this chapter and from Figure 5.1, it can be seen that the overall objective is to minimize the H_∞ norm of the transfer function from **w** to **z**.

The first step of this analysis is to obtain the general plant P. However, in order to get a meaningful controller synthesis, it is necessary to include the weights $\mathbf{w}_u$ for penalizing the control inputs, $\mathbf{w}_p$ for performance and $\mathbf{w}_T$ to ensure robust performance, as shown in figure 5.2 below.

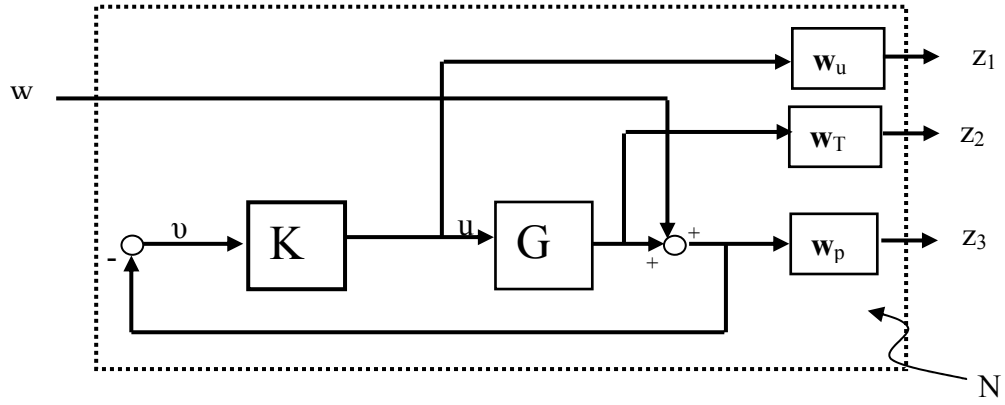

Figure 5.2.General plant including performance weights

The plant in Figure 5.2 is basically what will be used for solving the mixed sensitivity problem for controlling the satellite's orbit.
In the case of the satellite, an important consideration is to bound $\bar{\sigma}(S)$ for performance, $\bar{\sigma}(T)$ for robustness and $\bar{\sigma}(KS)$ to penalize large control inputs.

As mentioned previously, the above requirements can be combined to a mixed sensitivity problem, trying to find an optimal controller by solving

$$\min_K \left\| N(K) \right\|_\infty \quad \text{where} \quad N = \begin{bmatrix} \mathbf{w}_u KS \\ \mathbf{w}_T T \\ \mathbf{w}_P S \end{bmatrix}$$

It will be shown in the next part of this chapter that by solving the mixed sensitivity problem formulated here, an input multiplicative uncertainty which is my main interest in this case is included.

It can be seen from Figure 5.2 that *N* is the complete block. In order to obtain *N* we first need to derive the general plant *P*.

5.4.1 Obtaining the generalized plant *P*.

P is the open loop transfer function from $[\mathbf{w}\ \mathbf{u}\ ]^T$ to $[\ \mathbf{z}\ \boldsymbol{\upsilon}]^T$

Then, $$P = \begin{bmatrix} 0 & \mathbf{w}_u I \\ 0 & \mathbf{w}_T G \\ \mathbf{w}_p I & \mathbf{w}_p G \\ -I & -G \end{bmatrix} \qquad 5.20$$

In order however, to get *N, P* is needed to be partitioned as $P = \begin{bmatrix} P_{11} & P_{21} \\ P_{12} & P_{22} \end{bmatrix}$

Finally, by closing the loop, we have that $\mathbf{z} = N\mathbf{w}$ where N is given by

$$N = P_{11} + P_{12}K(I - P_{22}K)^{-1}P_{21} \triangleq F_l(P,K) \qquad 5.21$$

where, $F_l(P,K)$ denotes a lower *linear fractional transformation* (LFT) of *P* with *K* as a parameter.

In the case of the satellite's model, *P* was derived by using the MATLAB function

```
[P] = augtf(Gg, W1, W2, W3)
```

where G_g is the scaled general plant for the equations of motion of the satellite.

5.5. Control configuration including model uncertainty.

Model uncertainties, can be defined as the differences between the actual system and the system which was used to design. A control system is then robust if is insensitive to those differences.

The general NΔ structure is shown in Figure 5.3 below.

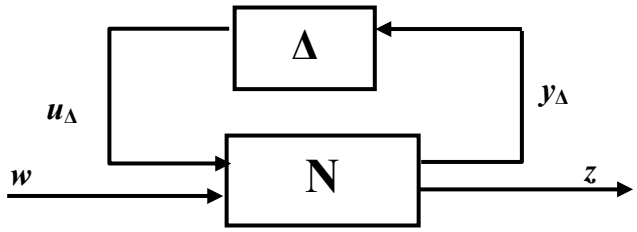

Figure 5.3.Uncertainty block in the general configuration.

For the robustness analysis, a system representation is used where the uncertain perturbations are "pulled out" into a block diagonal matrix as shown in Figures 5.4a and b below.

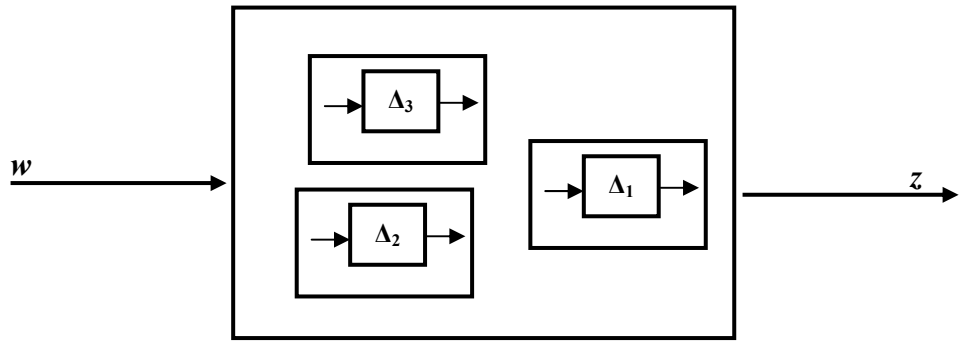

Figure5.4.a.Original system with multiple perturbations

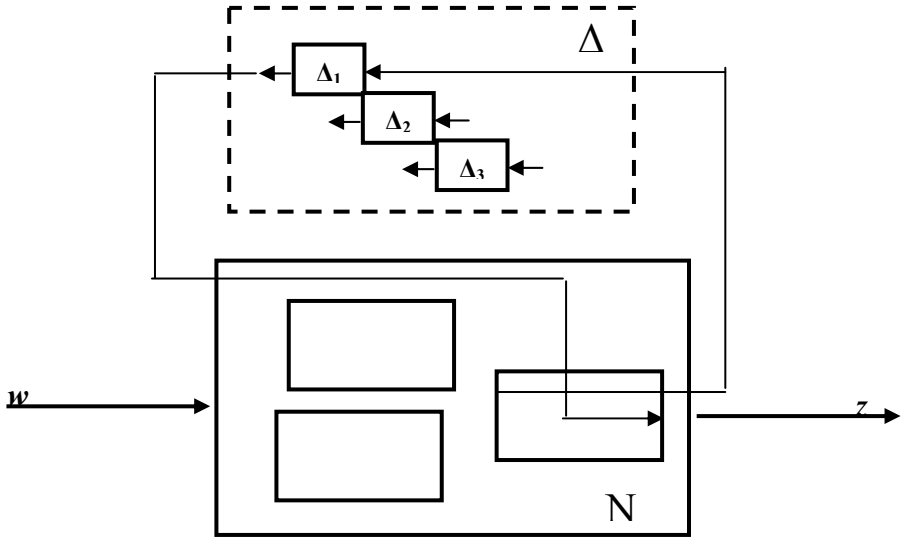

Figure 5.4.b. Pulling out the perturbances

As mentioned above N is related to P and K by a lower (LFT)

$$N = P_{11} + P_{12}K(I - P_{22}K)^{-1}P_{21} \triangleq F_l(P,K)$$

Similarly, the uncertain closed-loop transfer function from the input **w** to the output **z** is related to N and Δ by an upper (LFT)

$$F = N_{22} + N_{21}\Delta(I - N_{11}\Delta)^{-1}N_{12} \triangleq F_u(N,\Delta) \qquad 5.22$$

For analyzing robust stability of F the system is then re-arranged into the $M\Delta$ structured, where $M = N_{11}$ as shown in Figure 5.5 below.

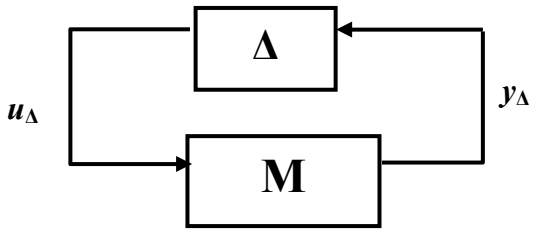

Figure 5.5.$M\Delta$ structure.

Each perturbation in the Δ structure, is assumed to be stable and normalized such as

$$\bar{\sigma}(\Delta_i(j\omega)) \le 1 \ \ \forall\omega, \forall i \ \ \Leftrightarrow \ \ \|\Delta\|_\infty \le 1 \qquad 5.23$$

5.5.1 Unstructured uncertainty.

Unstructured uncertainty can be defined as a full complex perturbation matrix Δ, where at any frequency, equation 5.23 is satisfied.

There are basically six common forms of unstructured uncertainties.
These are:
Additive and inverse additive uncertainty
Multiplicative and inverse multiplicative input uncertainty
Multiplicative and inverse multiplicative output uncertainty.

In the case of the control of the satellite, what is important and will be considered is the multiplicative input uncertainty for the reason that we are not absolutely sure what the output of the thrusters will be. The multiplicative input uncertainty is shown in Figure 5.6 below.

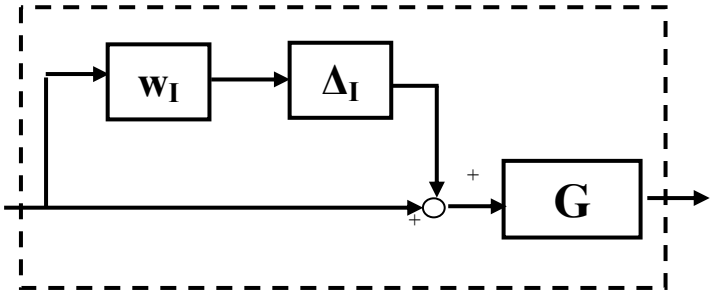

Figure 5.6.Multiplicative input uncertainty.

Then the perturbed plant, becomes:

$$G_P = G(I + E_I) \qquad \text{where} \qquad E_I = \mathbf{w}_I \Delta_I \tag{5.24}$$

5.5.2 Robust stability with multiplicative uncertainty.

In order to ensure robust stability in the case that multiplicative uncertainty is applied to the system, the following analysis occurs [11]

$$\left|\mathbf{w}_I L\right| \le \left|1 + L\right|, \forall \omega \tag{5.25}$$

$$\Rightarrow \quad \left|\frac{\mathbf{w}_I L}{1 + L}\right| \le 1, \quad \forall \omega \Leftrightarrow \left|\mathbf{w}_I T\right| < 1, \quad \forall \omega \quad \Leftrightarrow \left\|\mathbf{w}_I T\right\|_\infty < 1 \tag{5.26}$$

Finally, for RS in SISO systems $|T| < 1/|\mathbf{w}_I T|, \forall \omega$ 5.27

In the case of MIMO system, which is the case of the satellite's plant, the following theorem stands for unstructured uncertainties [11].

Assuming that the nominal system $M(s)$ is stable and that the perturbations $\Delta(s)$ are also stable, then the $M\Delta$ system of Figure 5.5 is stable for all perturbations Δ satisfying $\|\Delta\|_\infty < 1$

In other words, we have RS if and only if

$\bar{\sigma}(M(j\omega)) \le 1 \ \ \forall \omega, \forall i \ \ \Leftrightarrow \ \ \|M\|_\infty \le 1$ 5.28

Then, for the multiplicative uncertainty of Figure 5.6, we can assume that

$E = \mathbf{w}_2 \Delta_I \mathbf{w}_1, \quad \|\Delta\|_\infty \le 1$, since now we are considering a MIMO system.

To derive the matrix **M** the perturbation is isolated, and thus

$\mathbf{M} = \mathbf{W_1} M_o \mathbf{W}_2$ 5.29

Where, M_o is the transfer function from the output to the input of the perturbation.

For the case of the multiplicative uncertainty in the input,

$M_0 = K(I + GK)^{-1} G = T_I$ 5.30

Then from the theorem above, we get that

$\|W_1(j\omega) M_0 W_2(j\omega)\|_\infty \le 1 \quad \forall \omega$ 5.31

Then if we consider a multiplicative uncertainty with a scalar weight

$G_P = G(I + \mathbf{w}_I \Delta_I)$, $\|\Delta_I\|_\infty \le 1$

$\Rightarrow$ For RS we have $\|\mathbf{w}_I T_I\|_\infty \le 1$ 5.32

It can be seen here that equation 5.27 for SISO system is a special case of 5.32

5.5.3 Robust performance.

As mentioned previously, for having nominal performance the condition is

$$\left|\mathbf{w}_P S\right| < 1 \quad \forall \omega \quad \Leftrightarrow \quad \left|\mathbf{w}_P\right| < \left|1 + L\right|, \forall \omega \qquad 5.33$$

If we define again $L_P = G_P K$, then from equation 5.24 for multiplicative input uncertainty, we have:

$$L_P = L + \mathbf{w}_i L \Delta \qquad 5.34$$

What is required for robust performance (RP) is that the condition 5.33 is satisfied for all possible plants.

Then, if we define $S_P = (1 + L_P)$ for RP we get:

$$\begin{aligned} &\left|\mathbf{w}_P S_P\right| < 1 \quad \forall S_P, \omega \\ &\text{or, } \left|\mathbf{w}_P\right| < \left|1 + L_P\right| \end{aligned} \qquad 5.35$$

Therefore, from equations 5.24, 5.34 and 5.35, we can finally get that:

For RP

$$\begin{aligned} &\left|\mathbf{w}_p\right| + \left|\mathbf{w}_I L\right| < \left|1 + L\right| \quad , \forall \omega \\ &\Rightarrow \left|\mathbf{w}_p (1 + L)^{-1}\right| + \left|\mathbf{w}_I L (1 + L)^{-1}\right| \quad , \forall \omega \end{aligned} \qquad 5.36$$

Finally, for SISO systems, in order to ensure RP we have:

$$\max_\omega \left(\left|\mathbf{w}_p S\right| + \left|\mathbf{w}_I T\right| \right) < 1 \qquad 5.37$$

For Robust Performance on MIMO systems the structured singular value μ is introduced. One simple statement to define μ is: If we find the smallest structured Δ (measured in terms of $\bar{\sigma}(\Delta)$) which makes det(I-$M\Delta$) = 0 ,

then $\mu(M) = 1 / \bar{\sigma}(\Delta)$ 5.38

In MIMO systems, RP condition is the same as the RS only with an additional perturbation block Δ_P.

From the next theorem [11] which states that from the $N\Delta$ structure of Figure 5.3, if we assume nominal stability such as N is internally stable, then for RP

$$\|F\|_\infty = \|F_u(N,\Delta)\|_\infty < 1 \quad , \forall \|\Delta\|_\infty \le 1 \qquad 5.39$$

$$\Rightarrow \text{For RP in MIMO systems, } \mu_{\hat{\Delta}}\left(N(j\omega)\right) < 1 \text{ , } \forall\omega \qquad 5.40$$

where μ is computed with respect to the structure $\hat{\Delta} = \begin{bmatrix} \Delta & 0 \\ 0 & \Delta_p \end{bmatrix}$ and Δ_P is a full complex perturbation with the same dimensions as F

5.6. The satellite's control problem.

From the above analysis, it can be concluded that a good approach for solving the problem of controlling the satellite's orbit would be to try and find an optimal controller by minimizing the $H\infty$ norm of the transfer function of the inputs w to the outputs z as shown in Figure 5.2.

With the proper selection of weights the configuration of Figure 2 can be seen as in the model a multiplicative input uncertainty is considered since from equation 5.11 in order to ensure robust stability we need $\|\mathbf{w}_I T_I\|_\infty \le 1$.

The optimal controller was calculated by using the MATLAB function

```
[gamopt, sscp, sscl] = hinfopt(P)
```

where P is the generalize plant.

What is needed to be controlled in the satellite's case are the relative x, y and z. However those states are also the measured ones since with the use of the extended Kalman filter, we had very good estimations of those states.
This configuration can be considered as the optimum since what we want to control, can be measured with the help of the extended Kalman filter. The general configuration in MATLAB SIMULINK is shown in Figure 5.7 below.

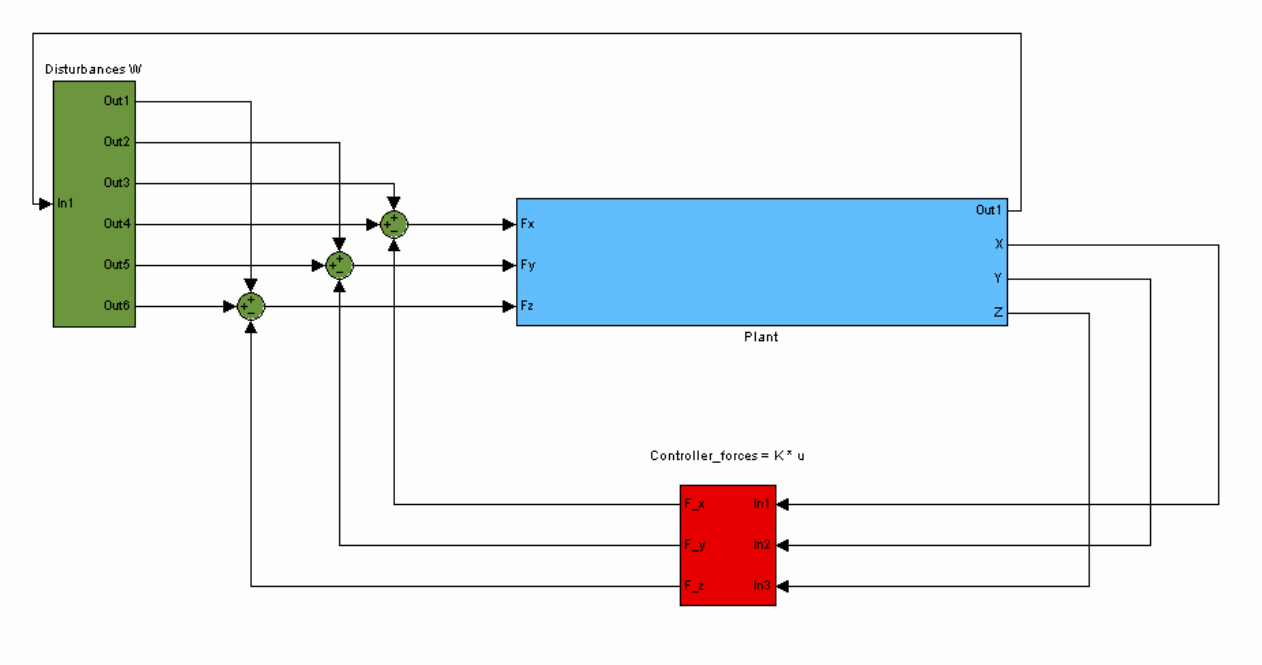

Figure 5.7 General configuration of the satellites model.

However, what has to be stated at this point is as mentioned previously, the system has six poles on the imaginary axis, causing calculation problems if `[gamopt, sscp, sscl] = hinfopt(P)` is used.

So, a solution to this problem was to add a small value e=0.1 in order to move the eigenvalues of the system to the right hand plane. This has not significant influence to the system and makes the calculations easier.

5.6.1 Selection of filter weights

As mentioned, all the previous analysis is a good indicator for choosing the initial weights. However for getting the final weights a lot of simulations were done and selected by trial and error. So the final weights are shown below:

5.6.1.1 Performance weight $\mathbf{w}_P$

$$\mathbf{w}_p(s) = \frac{s/M_s + \omega_B}{s + \omega_B A} \qquad 5.41$$

Where $\mathbf{w}_P$ is a diagonal matrix with components the scalar weights of equation 5.41

$M_s = 2$, A = 0.003 and $\omega_B = 10$ rad/s.

In Figure 5.8 below the singular values of the closed-loop transfer function $S = (I+L)^{-1}$ where $L = GK$ can be seen as well as the comparison with the singular values $1/\mathbf{w}_p$.

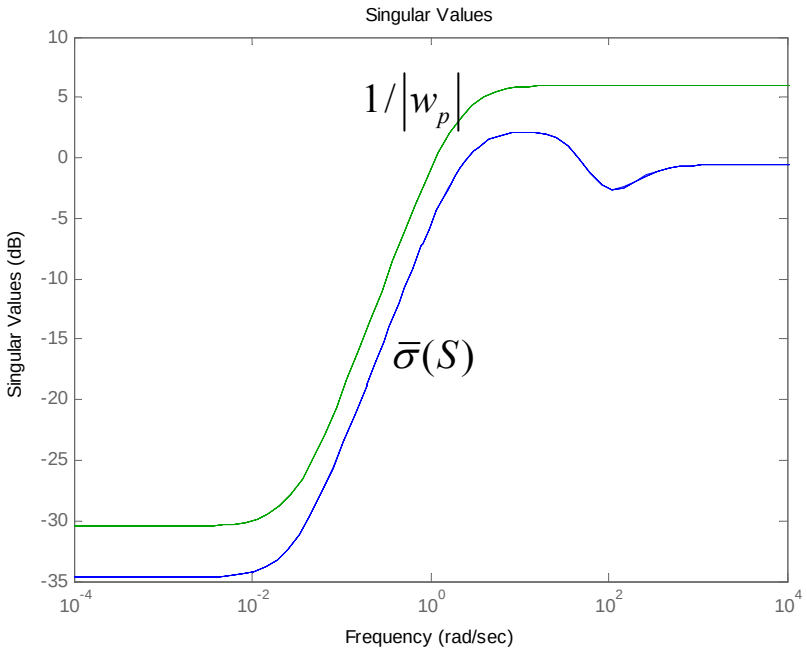

Figure 5.8.Singular values of $S = 1/(I+L)$ S compared with $1/\mathbf{w}_P$

5.6.1.2 Robustness weight $\mathbf{w}_I$

To represent unmodelled dynamics usually a simple multiplicative weight is used as shown in equation 5.42 below.

$$\mathbf{w}_I(s) = \frac{\tau s + r_0}{(\tau / r_\infty)s + 1} \qquad 5.42$$

where:

r_0 = the relative uncertainty at steady-state

$1/\tau$ = is (approximately) the frequency at which the relative uncertain reaches 100%

r_∞ = the magnitude of the weight at high frequency.

The final values of the filter $\mathbf{w}_I$ after a number of simulations are:

$r_0 = 0.3$

$\tau = 0.1$

$r_\infty = 2$

In Figure 5.9 below, the singular values of $T = ((1+L)^{-1} L)$ compared to the singular values of $1/\mathbf{w}_I$ are shown.

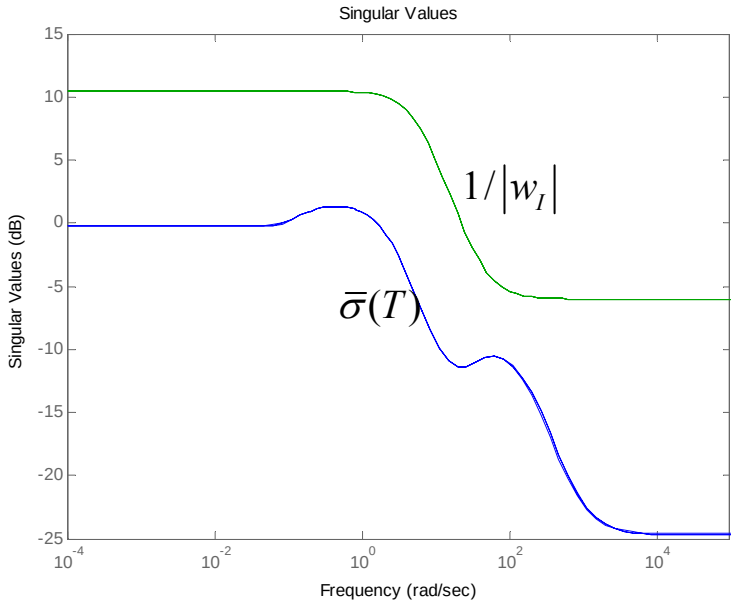

Figure 5.9.Singular values of $T = ((1+L)^{-1} L)$ compared to the singular values of $1/\mathbf{w}_I$

5.7 Final results

Finally, in the Figures below, the evolution of the states *x,y* and *z* relative are shown. The optimum control is to take the states to zero after the influence of the external disturbances caused by the sun, moon and the earth's non-homogeneous magnetic field. Then if the relative position of the satellite is $x = y = z = 0$, this means that the satellite will have the same position as the ideal point. The control of the satellite was made for 2880 minutes, which is equivalent to two days.

However, in the plots that follow only the first 200 minutes of the satellites trajectory are shown since there is not significant difference in any of the states after that period, and the results are clearer to see in this time scale. The initial conditions of the satellite were:
$x = y = z = 1\text{m}$

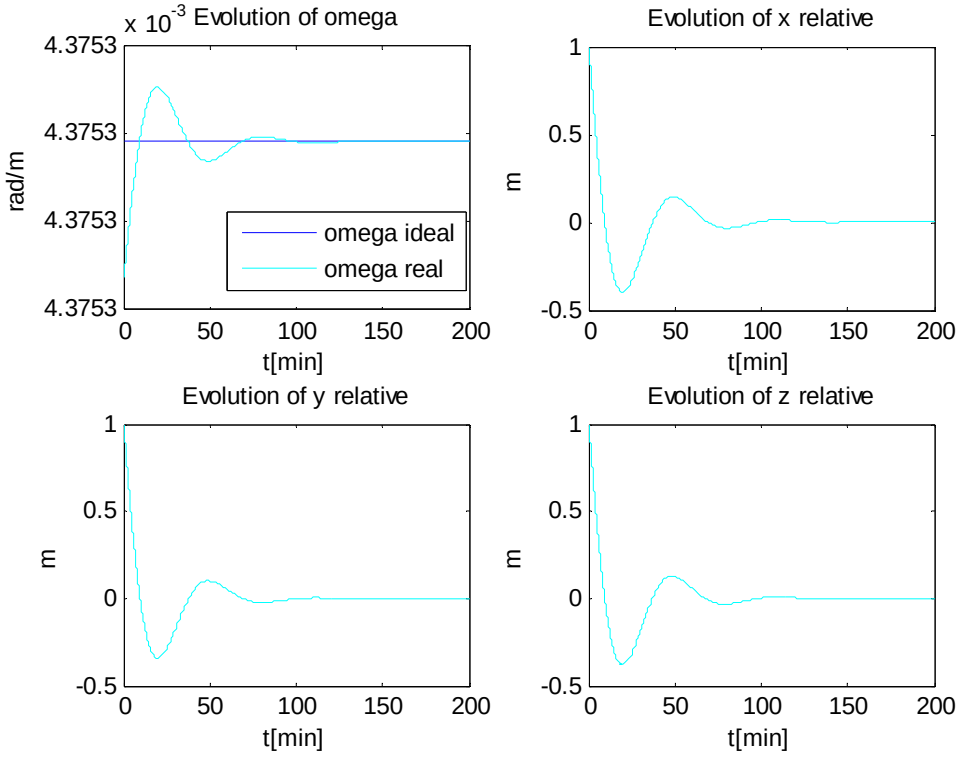

Figure 5.10.a omega ideal and omega real, evolution of *x* relative, evolution of *y* relative and evolution of *z* relative.

As can be seen in Figures 5.10 the error of the states goes fast to zero, which means that the controller is cancelling satisfactory the disturbances from the sun moon and earth.

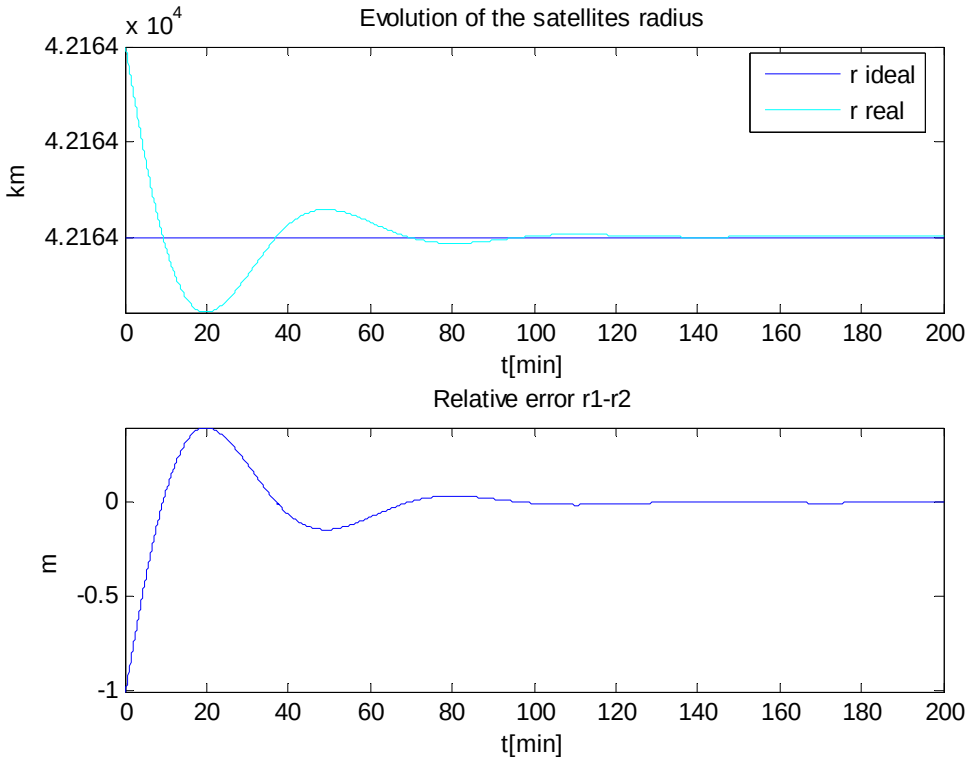

Figure 5.11.a Evolution of the satellites radius and the relative error.

Chapter 6
Comparisons and final conclusions

6.1. Introduction

Both of the control methods that were developed in the previous chapters, were tested with many simulations for different cases, such as for extreme initial conditions, high noise influencing the states of the system, and limited control signal after saturation was applied at the output of the controller. Both methods have very satisfactory results. However, those results were accomplished by analogous tuning for each case of the weights of the corresponding filters in the case of H_{inf} optimal controller and the weights of the corresponding matrices in LQR.

For example, when high gain to the weighting matrix **R** in the case of LQR or equivalently high gain to the weighting filter $\mathbf{w}_u$ was applied, for both cases then it took more time to the satellite to reach the desired position, but the fuel consumption was very low. But in the case of penalizing strongly the control input, if an additional noise was added to the states of the system, in both cases small oscillations were noticed. On the contrary, if the gain of the weighting filter $\mathbf{w}_u$ and the weighting matrix **R** was reduced, there were good results for robustness of the system, after the influence of noise, however the amount of fuel was considerably higher than the previous case.

So, the main conclusion of the many simulations with various cases is that both methods, with the proper "fine tuning" can have very good results, in every case independently. In order however, to compare these two methods, an imaginary scenario was created with some restrictions and both methods were tested and compared to this scenario. In each of the control method was applied after many trials what could be considered as the best selection of weighting filters and matrices in order to handle this scenario.

The results will be compared in respect to the total force applied to the satellite by each control method within the time window of 1000 minutes.

6.2. Comparison between the two control schemes.

As described in the introduction, an imaginary scenario will be implemented to test and compare the two optimization control methods.
What will be presented are the plots of the total forces given by the controller to the satellite, as well as the performance of the satellite.

The imaginary scenario, is described as follows: The satellites initial conditions would be $x_0 = y_0 = z_0 = 100$m and the maximum absolute value of force that can be applied to the satellite by the thrusters is of 100N. In addition, noise will be added to the states of the system that may be caused by interactions of the space environment to the satellites model such as solar pressure, or gravitational forces from other non modeled planets. Finally, the satellite should be within a boundary of ±10cm from the ideal point after a period of 100 minutes. For this test, the saturation limit will not be placed at the output of the controller since this will create a non-linearity to the system and then stability of the system can not be implied. However, what will be tested is if the corresponding force given by the two controllers is within the acceptable limits. If saturation is applied at the output the easiest way to prove the stability is by simulations since the controllers are designed for a linear system.

What will be used as a measurement of comparison is not the amount of fuel spent during the 1000 minutes but the integration of the force acted on the satellite, since as can be seen from Chapter 2.5 the fuel flow rate is analogous of the thruster force.

The equations of the thruster forces 2.27 and 2.28 are presented at this point again.

$$F = V_e \frac{dm}{dt} + A[P_e - P_a] \qquad 6.1$$

$$I_{sp} = F / \left(g \frac{dm}{dt} \right) \text{ measured in seconds} \qquad 6.2$$

6.2.1. LQ regulator optimal controller

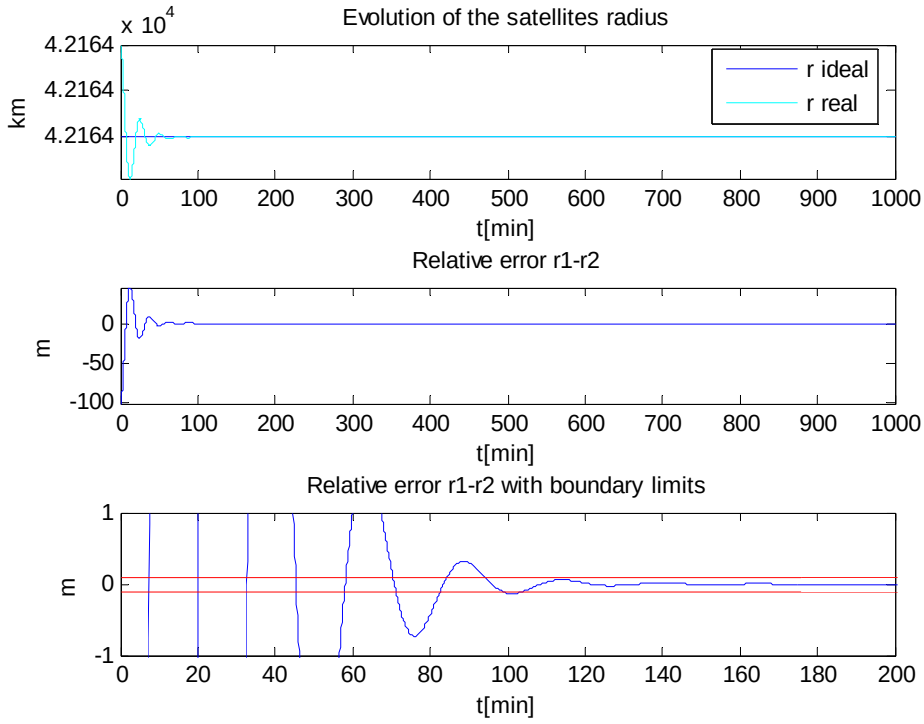

Figure 6.1.Evolution of the satellites radius, the relative error and the boundary condition for the case were the controller was designed by LQ regulator methodology.

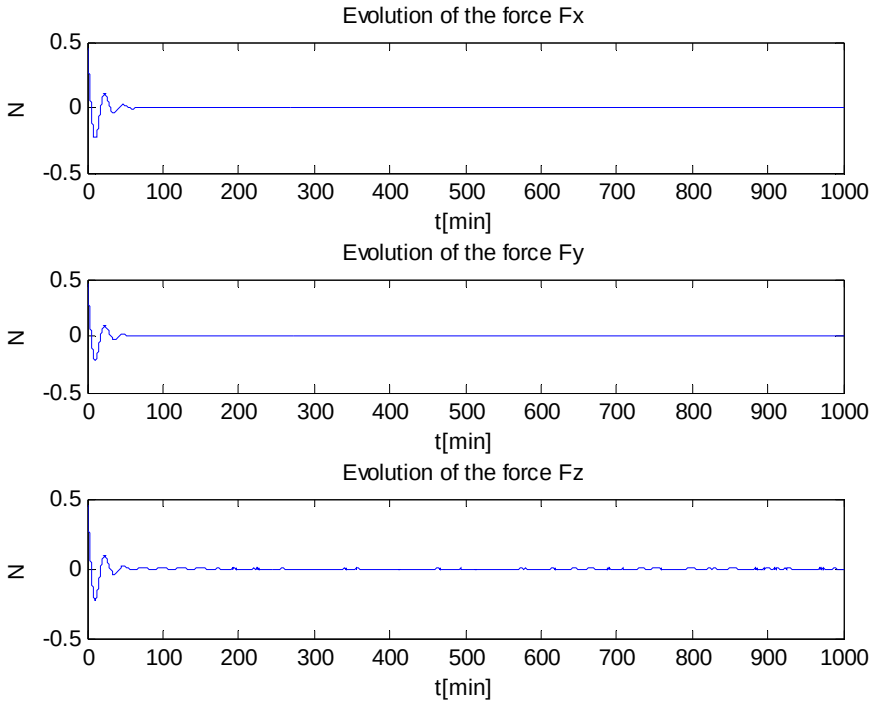

Figure 6.2.Evolution of the thruster forces F_x, F_y and F_z given by the LQ controller

In figure 6.1 what can be seen is the evolution of the satellites radius as well as how the satellite is within the boundary limit of ±10cm after 100 minutes. In addition Figure 6.2 shows the evolution of the forces in the three relative directions *x*, *y* and *z*.

Since the whole model is in discrete time, the integration of the total force acting in the *x, y* and *z* direction is equal to the total summation of the absolute value. The reason that an absolute value is used is because the negative force is equivalent with a force caused by the thruster in the opposite direction.

For the case of the LQ regulator in the time period of 100 minutes is:

$\boldsymbol{F_x}$ **= 0.6619 N ,** $\boldsymbol{F_y}$ **0.5869 N,** $\boldsymbol{F_z}$ **= 0.6260 N**

The total force acted on the satellite is:

$\boldsymbol{F_{total}}$ **= 1.8748 N**

The weighting matrices **Q** and **R** were selected as:

$$\mathbf{R} = \begin{bmatrix} 200 & 0 & 0 \\ 0 & 200 & 0 \\ 0 & 0 & 200 \end{bmatrix}, \qquad \mathbf{Q} = \begin{bmatrix} 1 & 0 & 0 & 0 & 0 & 0 \\ 0 & 1 & 0 & 0 & 0 & 0 \\ 0 & 0 & 1 & 0 & 0 & 0 \\ 0 & 0 & 0 & 1 & 0 & 0 \\ 0 & 0 & 0 & 0 & 1 & 0 \\ 0 & 0 & 0 & 0 & 0 & 1 \end{bmatrix} \tag{6.3}$$

6.2.2. H-Infinity Optimal Control

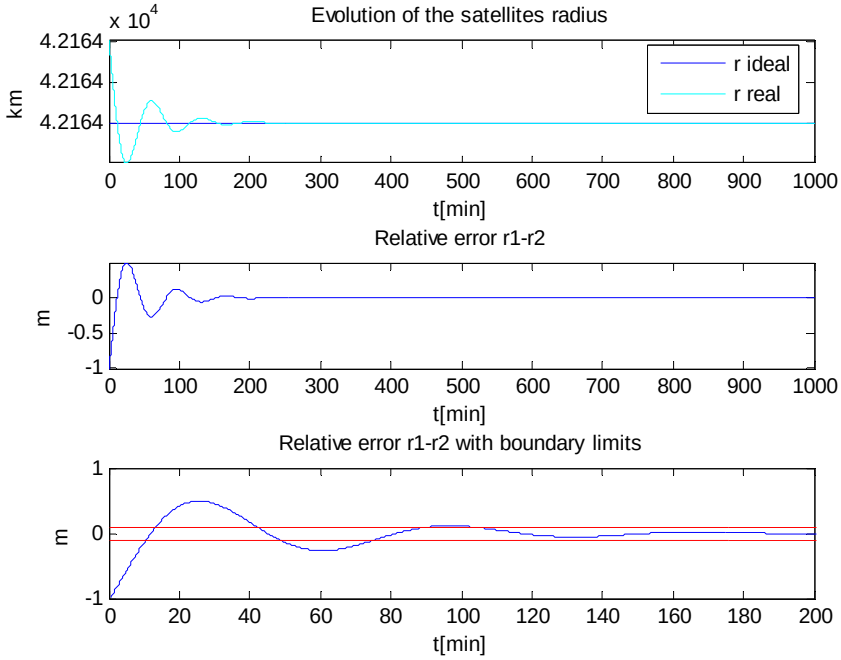

Figure 6.3.Evolution of the satellites radius, the relative error and the boundary condition for the case were the controller was designed by H_{inf} Optimal Control Synthesis.

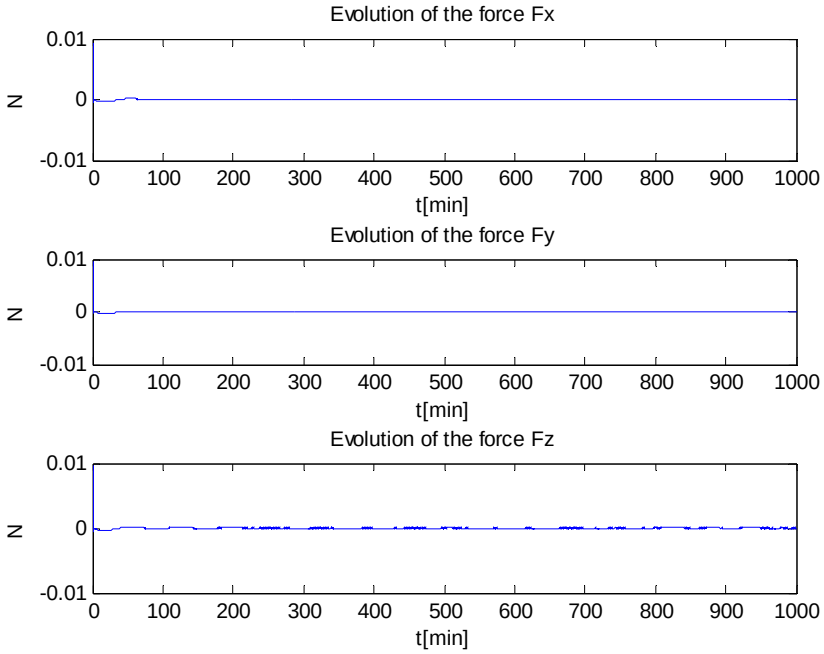

Figure 6.4.Evolution of the thruster forces F_x, F_y and F_z

The summation of the absolute value of the three forces given by the controller designed with H-Infinity Optimal Control Synthesis regulator in the time period of 100 minutes is:

F_x = 0.0060 N , F_y 0.0050 N, F_z = 0.0033 N

The total force acted on the satellite is:

F_{total} = 0.0143 N

The weighting filters $\mathbf{w}_p$, $\mathbf{w}_I$ and $\mathbf{w}_u$ were selected as shown below:

$$\mathbf{w}_p(s) = \frac{\frac{s}{M_s} + \omega_B}{s + \omega_B A} \qquad 6.4$$

where

$M_s = 2$, $A = 0.03$, $\omega_B = 1$ rad/s , and is applied the same for the three system outputs

$$\mathbf{w}_I(s) = \frac{\tau s + r_0}{(\tau / r_\infty)s + 1} \qquad 6.5$$

where

$\tau = 1/20$, $r_0 = 0.3$, $r_\infty = 2$, the same for the three outputs of the satellites plant

And $\mathbf{w}_u = 1.5$ the same for the three outputs of the controller. 6.6

6.2.3. Non-linear model tests.

As described previously in this chapter, if the control signal is saturated then the system has nonlinearities and the easiest way to prove the stability is by simulations. Additionally, with the assumptions made in chapter 1 in order to derive the linear equations of motion the satellite should be near the ideal point. So, by taking large initial conditions the assumption does not stand.

In the figures that follows, what is shown is the model simulated with initial conditions $x_0 = y_0 = z_0 = 1$km, with additional noise added to the system and the output of the controller to be saturated at 1 N.

6.2.3.1 LQ regulator optimal controller

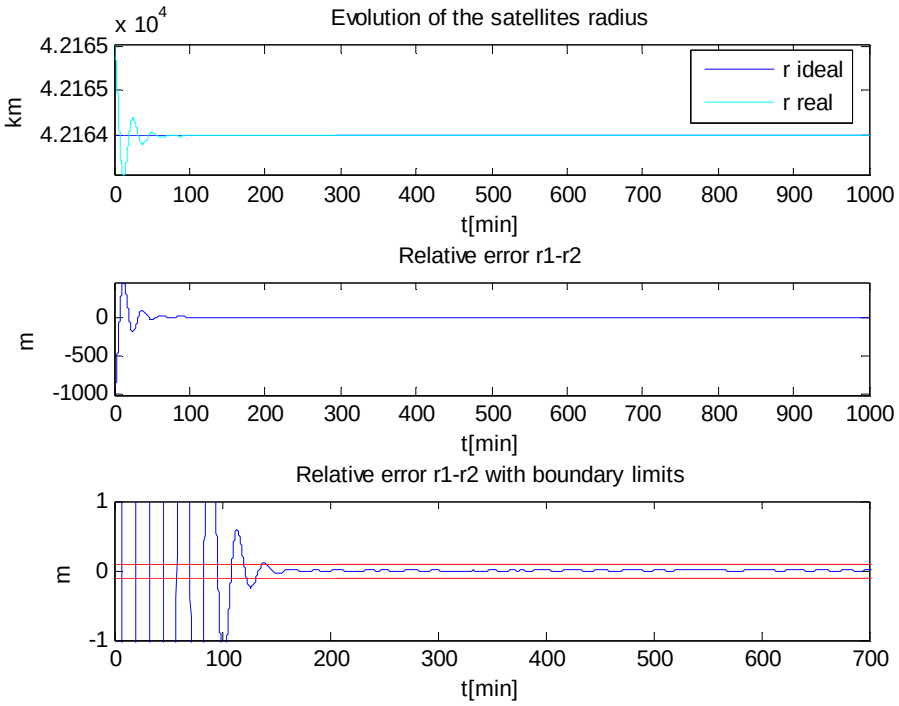

Figure 6.5.Evolution of the satellites radius, the relative error with the control signal saturated and initial conditions of 1km by LQR Optimal Controller.

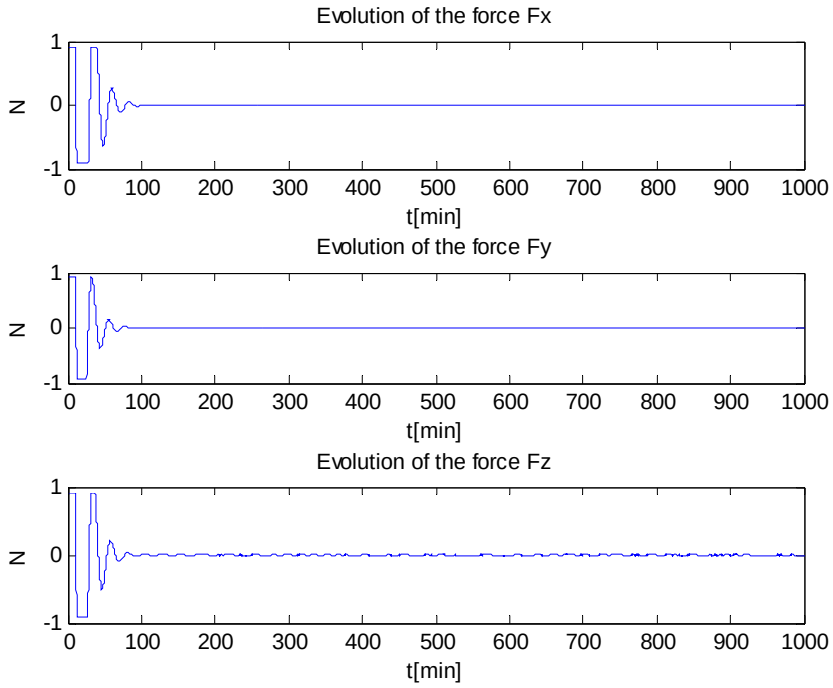

Figure 6.6.Evolution of the thruster forces F_x, F_y and F_z with control signal saturated.

6.2.3.2 H-Infinity Optimal Control

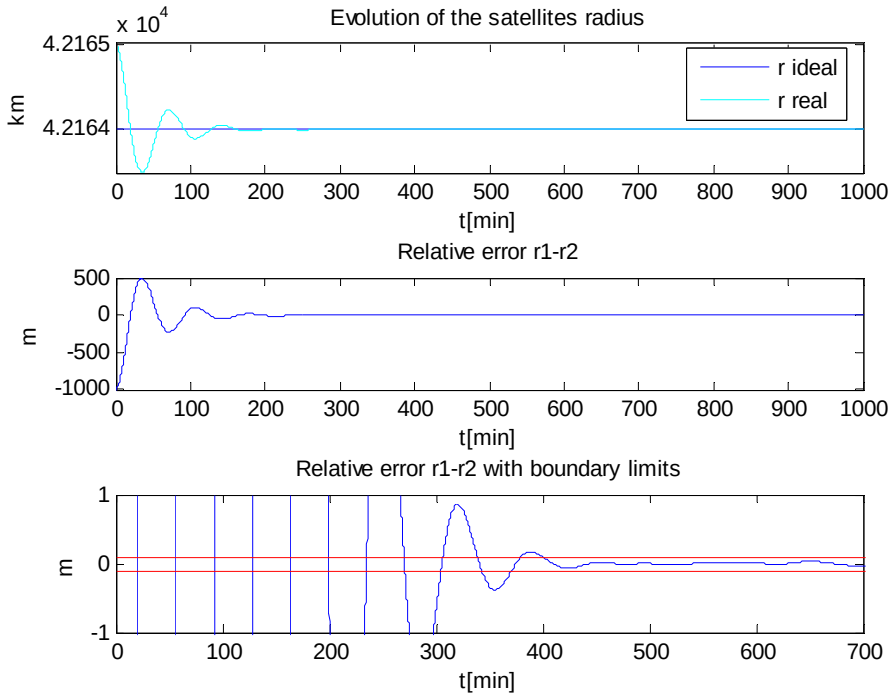

Figure 6.7.Evolution of the satellites radius, the relative error with the control signal saturated and initial conditions of 1km by H_{inf} Optimal Control Synthesis.

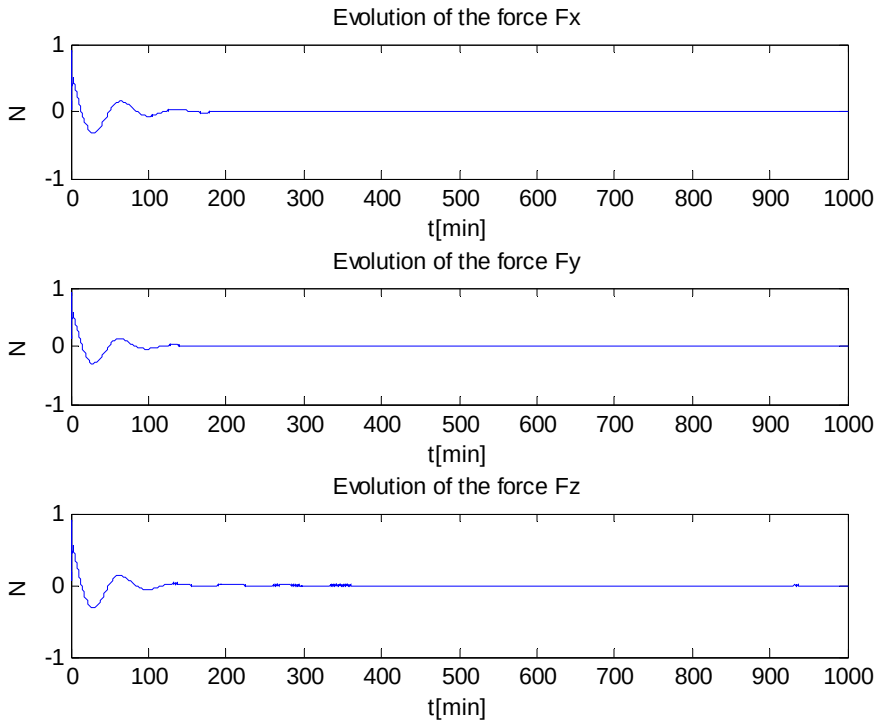

Figure 6.8.Evolution of the thruster forces F_x, F_y and F_z with control signal saturated.

6.3 Conclusions.

After many simulations with different values for the weighting matrices and filters, as well as many different cases the conclusions are that basically both methods with the proper design and tuning can have very good results in the specific case.

The basic differences in the special case of the imaginary scenario that I observed is that as far as robustness concern, the H_{inf} controller is more reliable. Even with higher noise it could still stabilize the satellite still with low fuel consumption. In order for the controller given by the LQ regulator methodology, to stabilize the satellite when high noise was applied to the system, the weighting matrix **Q** had to become very large.

This can also be confirmed if the Figures 6. 1, 2, 3 and 4 are observed when both methods were tested in the scenario described previously. The total force applied to the satellite within 100 minutes with the H_{inf} controller its much less than that given by the LQR. Nevertheless, the above conclusions are applied specifically for the case of the scenario described and should not be considered as a general case since with proper tuning of the weighting matrices, LQ controller can have equally good results.

Another conclusion that was derived from the simulations that had been made is that even if the output of both of the controllers was saturated, and the initial conditions were set very far away from the ideal point, the satellite was still stabilized. On the other hand, what can be noticed is that with both control methods, additional oscillations occurred. The problem with the oscillations caused by the saturation of the control signal can be solved with two methods. The first method would be to add anti-wind strategy to the controller [14] .This method basically stops the operation of the integrator at the point where the signal is saturated [15].

The second way to solve this problem would be by using a Model Predictive Control (MPC). The main idea of MPC is to choose the control action by repeatedly solving on line an optimal control problem. The online optimization problem takes account of system dynamics, constraints and control objectives. Conventional model predictive control requires the solution of an open-loop optimal control problem, in which the decision variable is a sequence of control actions, at each sample time. This aims at minimizing a performance criterion over a future horizon and most of the time when it is subject to constraints on the manipulated inputs and outputs [16]. For more information about Model Predictive Control, a number of references can be found on the webpage: http://www.rpi.edu/dept/chem-eng/WWW/faculty/bequette/courses/mpc/MPC_refs.pdf.

As for designing of the controllers, there are advantages and disadvantages in both methods. With the H_{inf}, the controller has some dynamics and probably is more difficult to be designed while with LQ, the controller is only a gain. The advantage though of the H_{inf} controller that has been studied in this case, is that it takes as inputs only the three states which this makes it easier to adapt it in the satellite since there is not a lot of information needed. On the other hand, the LQ controller it's designed to have full state feedback.

7. Bibliography

[1] Sidi M. J. (1997). **Spacecraft Dynamics and Control**. Cambridge.

[2] Schweighart S. A. (2001). **Development and Analysis of a High Fidelity Linearized J2 Model for Satellite Formation Flying**. MSc Thesis. MIT.

[3] Willey J. L., James R. W. (1999). **Space Mission and Analysis**. Springer – Verlag.

[4] Professor Guelman, **Lecture notes in formation flight**. University of Wuerzburg, Erasmus Mundus SpaceMaster Course.

[5] Anderson B. D., Moore J. B. (2005). **Optimal Filtering**, Dover Publications.

[6] Lewis F. L., Syrmos V. L. (1995). **Optimal Control**. 2nd edition. John Wiley & sons.

[7] Online slides (http://www.stanford.edu/class/ee363)

[8] Franklin G. F., Powell J. D., Emami-Naeini A. (2002). **Feedback Control of Dynamic Systems**. Prentice-Hall.

[9] Roubal J., Augusta P., a Havlena V. (2005). **A Brief Introduction to Control Design Demonstrated on Laboratory Model Servo DR300** –Amira. Acta Electrotechnica et Informatica, No. 5, Vol. 4, 2005.

[10] MATLAB tutorial of **Robust Control Toolbox**.

[11] Skogestad S., Postletwaite I. (2005). **Multivariable Feedback Control, Analysis** and Design. Wiley.

[12] Boyd S. **Linear Dynamic Systems**. (http://www.ist.uni-stuttgart.de/)

[13] Professor Hurák. **Lecture notes on Optimal and robust control design**.

[14] Navneet K., Andrew R. T., Daoutidis P. (1998). **An anti-windup design for linear systems with input saturation.** Automatica v.34 n.5**,** p.559-574, May 1, 1998.

[15] Gomes da Silva M. Jr, Tarbouriech S., Reginatto R. (2002). **Analysis of regions of stability for linear systems with saturating inputs through an anti-windup scheme**. Proceedings of the IEE Conference on Control Applications (CCA), Glasgow, Scotland, 2002, p. 1106-1111.

[16] Roubal J.(2006). **Model Predictive Control of~2D~Systems.** Ph.D.Thesis, Czech Technical University, Prague.